Geol. Mag. **140** (*4*), *2003, pp. 397–420.* © *2003 Cambridge University Press*
DOI: 10.1017/S0016756803007830 *Printed in the United Kingdom*

Changes in organic matter production and accumulation as a mechanism for isotopic evolution in the Mesoproterozoic ocean

T. D. FRANK*, L. C. KAH† & T. W. LYONS‡

*Department of Earth Sciences, University of Queensland, St Lucia QLD 4072, Australia
†Department of Geological Sciences, University of Tennessee, Knoxville TN 37996, USA
‡Department of Geological Sciences, University of Missouri, Columbia MO 65211, USA

(*Received* 28 February 2002; *revised version received* 24 February 2003; *accepted* 20 March 2003)

Abstract – Mesoproterozoic marine successions worldwide record a shift in average $\delta^{13}C$ values from 0 to +3.5 ‰, with the latter value evident in successions younger than 1250 Ma. New carbon isotope data from the ~1300 to 1270 Ma Dismal Lakes Group, Arctic Canada, provide further insight into this fundamental transition. Data reveal that the shift to higher $\delta^{13}C$ values was gradual and marked by occasional excursions to values less than 0 ‰. When compared to records from older and younger marine successions, it is evident that the difference between isotopic minima and maxima increased with time, indicating that the marine system evolved to become isotopically more variable. We interpret these patterns to record an increase in the crustal inventory of organic carbon, reflecting eukaryotic diversification and a change in the locus of organic carbon burial to include anoxic deep marine sites where preservation potential was high. We speculate that the release of O_2 to Earth's surface environments associated with increased organic carbon storage induced irreversible changes in the Mesoproterozoic biosphere, presaging the more extreme environmental and evolutionary developments of the Neoproterozoic.

Keywords: Mesoproterozoic, carbonate rocks, C-13/C-12, chemostratigraphy, carbon cycle.

1. Introduction

Much emphasis has been placed on understanding the nature of biogeochemical processes during Neoproterozoic time, particularly between *c*. 800 and 550 Ma. This interval was marked by a fluctuating marine $\delta^{13}C$ record (Kaufman & Knoll, 1995, and references therein), vacillation between global climate extremes (Kaufmann, Knoll & Narbonne, 1997; Hoffman, Kaufman & Halverson, 1998; Hoffman *et al*. 1998), diversification of multicellular algal communities (Zhang & Yuan, 1996; Woods, Knoll & German, 1998; Xiao, Knoll & Yuan, 1998; Xiao, Zhang & Knoll, 1998), the appearance of the Ediacaran fauna (Fedonkin, 1990; Knoll & Walter, 1992; Narbonne, Kaufman & Knoll, 1994; Grotzinger *et al*. 1995; Narbonne, 1998) and the advent of metazoan mineralization (Braiser, Green & Shields, 1997; Grotzinger, Watters & Knoll, 2000). By contrast, our understanding of conditions leading up to the Neoproterozoic is relatively limited.

The Mesoproterozoic Eon (1600 to 1000 Ma) represents a critical period in Earth history from the standpoint of global tectonic reorganization (Hoffman, 1989, 1991; Dalziel, 1991; Karlstrom *et al*. 2001), the redox state of the oceans (Des Marais *et al*. 1992; Canfield & Teske, 1996; Canfield, 1998), the carbonate saturation state of the oceans (Grotzinger, 1989; Kah & Knoll, 1996; Bartley *et al*. 2000; Kah, Lyons & Chesley, 2001), eukaryotic diversification (Knoll, 1992; Anbar & Knoll, 2002) and the advent of multicellularity (Butterfield, Knoll & Swett, 1990; Woods, Knoll & German, 1998; Butterfield, 2000). Only recently, however, have enough geochemical data that are well-constrained in terms of age, depositional environment and post-depositional history become available to permit the evaluation of even first-order secular variation in the marine carbon isotope system (Buick, Des Marais & Knoll, 1995; Knoll, Kaufman & Semikhatov, 1995; Xiao *et al*. 1997; Frank, Lyons & Lohmann, 1997; Kah *et al*. 1999*a*; Lindsay & Braiser, 2000; Bartley *et al*. 2001). Whereas previous workers have described the Mesoproterozoic $\delta^{13}C$ record as uneventful (Buick, Des Marais & Knoll, 1995; Brasier & Lindsay, 1998), a more recent and extensive compilation of data (Kah *et al*. 1999*a*) indicates that the Mesoproterozoic can be divided into two distinct intervals based on the variation and magnitude of $\delta^{13}C$ values in the marine carbonate record. Marine carbonates of early Mesoproterozoic age exhibit uniform carbon isotope compositions ($\delta^{13}C = 0.0 \pm 1.0$ ‰), consistent with prolonged stability of the marine carbon cycle between 1600 and ~1300 Ma. Carbonate strata younger than ~1200 Ma are characterized by higher $\delta^{13}C$ values ($\delta^{13}C = +3.5 \pm 1.0$ ‰). The shift

* Author for correspondence: tfrank2@unl.edu; present address: Department of Geosciences, University of Nebraska, Lincoln, NE 68588-0340, USA.

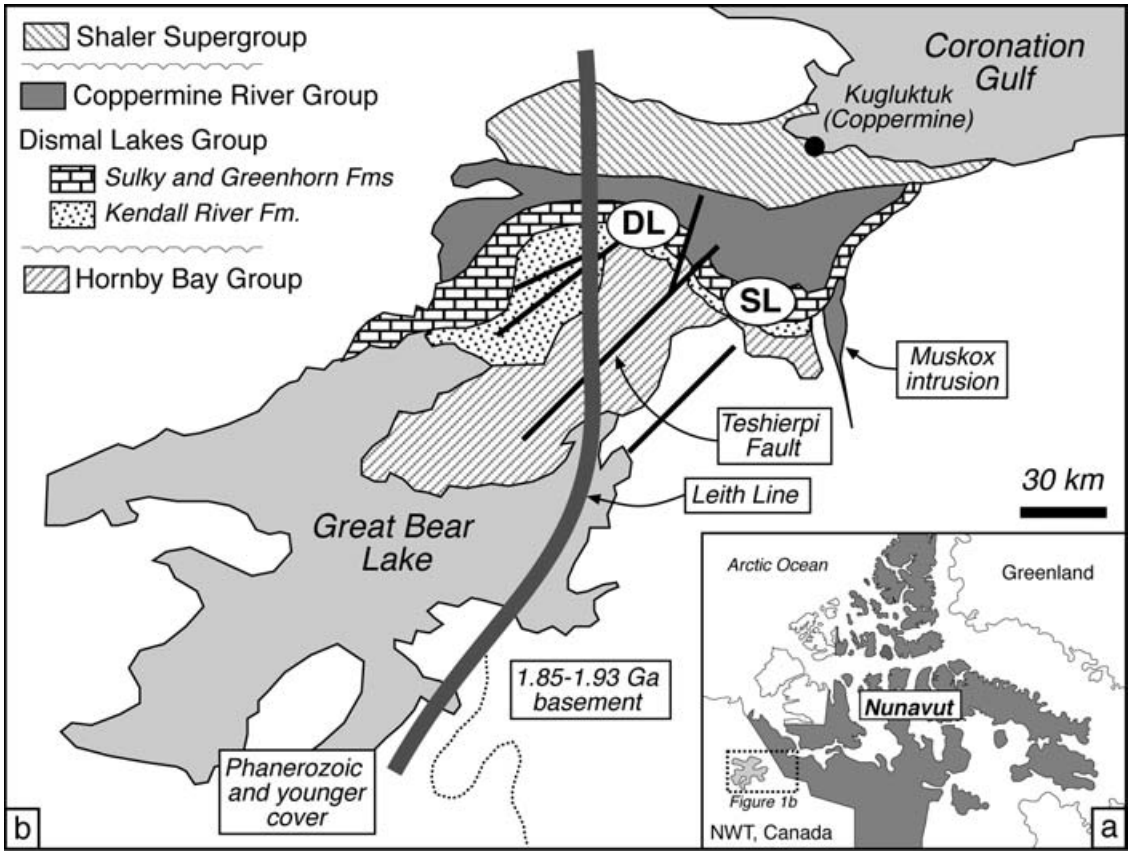

Figure 1. Geological map of the Coppermine Homocline, modified from Kerans *et al*. (1981) and Ross & Kerans (1988), showing outcrop extent of the Dismal Lakes Group and major basement features. Reactivation of the Leith Line and Teshierpi Fault during Dismal Lakes deposition significantly affected basin development. Samples for isotopic analysis were collected from measured sections in the region of September Lake (SL) and north of Dismal Lake (DL).

to higher $\delta^{13}C$ values suggests a fundamental change in ocean chemistry, which persisted throughout the latter half of the Mesoproterozoic. Although it is clear that these first-order variations are of broad chronostratigraphic utility (Kah *et al*. 1999*a*; Bartley *et al*. 2001), additional data are needed to constrain more precisely the timing and nature of this carbon isotope transition and to interpret its significance with regard to global-scale processes.

In this paper we present new carbon isotope data from the Dismal Lakes Group, Arctic Canada, which was deposited *c*. 1300–1270 Ma, during the global shift in marine carbon isotope composition from 0‰ to 3.5‰ reported in Kah *et al*. (1999*a*). Five detailed sections through Dismal Lake carbonate strata were measured in the regions of September Lake and Dismal Lake (Fig. 1). Depositional facies record a variety of water depths ranging from marine peritidal to mid-shelf environments (Kerans *et al*. 1981; Kerans, 1983; Kerans & Donaldson, 1988, 1989). Samples for petrographic and geochemical analysis were collected at 5–10 m intervals from each measured section and all depositional facies, providing an opportunity to examine both temporal (that is, stratigraphic) change in ocean chemistry, as well as regional variations related to basin-scale processes. We use an integrated approach, in which geochemical data are evaluated for possible diagenetic effects and interpreted within a petrographic, sedimentological and stratigraphic framework. This approach permits evaluation of diagenetic trends and recognition of primary isotopic signatures, and ultimately aids in resolving global versus local influences on isotopic variation. Comparisons of resulting data with those from Mesoproterozoic successions worldwide are used to resolve the timing of the mid-Mesoproterozoic global carbon isotope transition and to evaluate the character of the shift with respect to its possible driving forces.

2. Geological setting and age

2.a. Regional geology

The N-dipping Coppermine Homocline, Northwest and Nunavut territories, Arctic Canada, is represented by >4000 m of unmetamorphosed and virtually undeformed siliciclastic, carbonate and volcanic rocks (Fig. 1). The homocline succession is composed of the predominantly sedimentary Hornby Bay and Dismal

Lakes groups and takes its name from the regionally extensive, extrusive volcanic rocks of the Coppermine River Group (Barager & Donaldson, 1973). Strata of the Coppermine Homocline unconformably overlie metamorphic and volcanic rocks of the Great Bear Batholith and McTavish Supergroup (Hildebrand, 1981), located in the northernmost extension of the Palaeoproterozoic (~1.93 to 1.85 Ga) Wopmay Orogen (Van Schmus & Bowring, 1980; Hoffman & Bowring, 1984). Coppermine strata are unconformably overlain by Phanerozoic cover and, in part, by carbonate and siliciclastic strata of the Neoproterozoic Rae Group, Shaler Supergroup (Young, 1979, 1981*a*, *b*; Rainbird *et al*. 1994; Rainbird, Jefferson & Young, 1996). Together, the Hornby Bay and Dismal Lakes groups record a complex history of post-Wopmay crustal stabilization (Kerans *et al*. 1981), episodes of compressional and extensional intracratonic adjustment (Kerans *et al*. 1981; Cook & MacLean, 1992, 1995, 1996), periods of tectonic stability (Kerans *et al*. 1981) and regional uplift (Kerans, 1983) prior to the extrusion of voluminous flood basalts of the Coppermine River Group.

2.b. Dismal Lakes Group

Within the Coppermine Homocline, the >1500 m thick Dismal Lakes Group is exposed in a sinuous belt stretching from Great Bear Lake to the Coronation Gulf (Fig. 1). Basin development during Dismal Lakes deposition was governed in part by reactivation of antecedent structural elements. Higher rates of subsidence to the west of a major structural hinge (Leith Line; Fig. 1) resulted in significant deepening and thickening of depositional units westward of the September Lake High (Fig. 2; Kerans *et al*. 1981). This effect was heightened by the reactivation of a series of NE-trending structures (e.g. Teshierpi Fault; Fig. 1) before and during Dismal Lakes deposition (Cook & MacLean, 1992, 1996). These faults originated as conjugate transcurrent faults during oblique convergence of the Wopmay Orogen (Hoffman, 1980*a*; Hoffman & St Onge, 1981).

The Dismal Lakes Group consists of the siliciclastic-dominated LeRoux, Fort Confidence and Dease Lake formations and the carbonate-dominated Kendall River, Sulky and Greenhorn formations (Fig. 2; Ross & Kerans, 1988). Basal strata consist of fluvial and marginal marine quartz arenites (Kerans *et al*. 1981). Siliciclastic mudstones, which show evidence of shallow-water deposition and subaerial exposure, become increasingly dominant in the Fort Confidence and Dease Lake formations and record the gradual development of a low-relief, siliciclastic shoreline (Kerans *et al*. 1981). In the overlying Kendall River Formation, siliciclastic facies gradually disappear, while oolitic, intraclastic and microbially laminated carbonates become increasingly prominent. This transition from siliciclastic- to carbonate-dominated facies records the development of the Dismal Lakes carbonate platform. The regional uniformity and lateral continuity of Kendall River carbonate facies (Kerans *et al*. 1981) suggest minimal activity along major structural elements (Teshierpi Fault and Leith Line) as the platform became established.

The overlying Sulky Formation contains three informal members (Kerans *et al*. 1981). East–west facies trends and increasing stratigraphic thickness to the west suggest that NE-trending structural elements became active during Sulky deposition. The lower Sulky member consists of structureless to parallel-laminated flaggy dolostones with thin interbeds of red and black shale. Soft-sediment slump structures and carbonate debris flows in strata to the west of the Leith Line indicate the development of a W-facing slope (Kerans *et al*. 1981). East of the Teshierpi Fault, the top of the lower Sulky member is marked by an unconformity with up to 5 m of erosional relief. To the west, in the region of Dismal Lake (Fig. 2), the contact between the lower and middle Sulky members is conformable, suggesting that subaerial exposure, related to uplift and/or a drop in relative sea level, was limited to the eastern (shallower) part of the basin.

Stratigraphic relationships and sedimentological data suggest that deposition of the middle Sulky member commenced during a rise in relative sea level. East of the Teshierpi Fault, this rise is marked by the development of the ~30 m thick September Lake reef complex, composed of massive, conical stromatolites that preserve a synoptic relief of greater than 10 m (Donaldson, 1976; Kerans *et al*. 1981; Kerans & Donaldson, 1989). The absence of reef debris between coniforms and the magnitude of synoptic relief suggest that the main stage of reef growth occurred in a low-energy depositional setting, likely below storm wavebase. Coniform stromatolites of the September Lake reef complex are overlain by massive domal to columnar forms, suggesting gradual shallowing (Kerans & Donaldson, 1989). West of the Teshierpi Fault, the middle Sulky member consists of a 4.1 m interval of finely laminated, organic-rich dolostone with unusual cuspate microbialite structures (flank facies of Kerans & Donaldson, 1989). These microbialites consist of an open network of draping laminae over thin, vertical supports and are similar to those reported in the Archean Transvaal Supergroup, South Africa (Sumner, 1997). Structural void space is filled with several generations of carbonate cement, including penecontemporaneous herringbone cements (cf. Sumner & Grotzinger, 1996*a*, *b*) and a late-stage purple, ferroan dolomite cement. Microbialite morphology, inferred palaeobathymetry and the close association with herringbone precipitates and organic-rich, finely laminated dolostone suggests that the microbialites formed in relatively deep, suboxic to anoxic waters (Kah *et al*. 1999*b*).

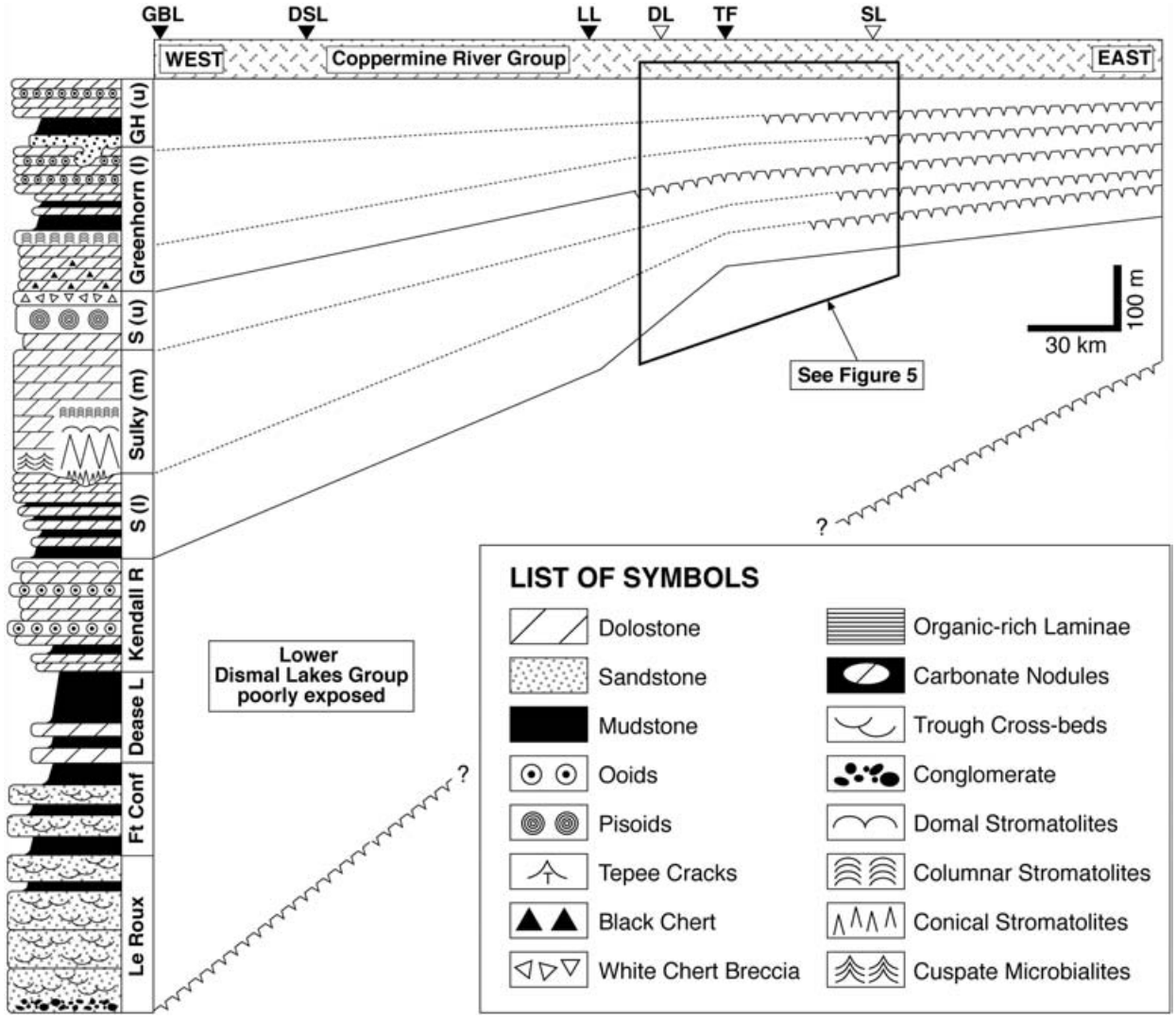

Figure 2. Generalized stratigraphy and cross-section of the Dismal Lakes Group, modified from Kerans *et al*. (1981). Lower, siliciclastic units are poorly exposed in the Coppermine Homocline, and likely overlie the Hornby Bay Group with significant disconformity (Cook & MacLean, 1992). Dramatic thickening of Dismal Lakes strata is recorded in the regions of Dease Lake (DSL) and Great Bear Lake (GBL) west of the antecedent Teshierpi Fault (TF) and Leith Line (LL). Type I sequence boundaries (showing subaerial exposure, incision and/or karst development) are common in Dismal Lakes Group carbonate strata, and are most pronounced on September Lake High, east of the Teshierpi Fault. Samples for chemostratigraphic analysis were collected from measured sections in the region of September Lake (SL) and Dismal Lake (DL). See Figure 5 for details of measured sections.

In the region of the September Reef Complex, the contact with the upper Sulky member is sharp and overlain by ~20 m of fenestral and pisolitic dolostone. West of the Teshierpi Fault, the upper Sulky comprises interbedded dolomicrites, quartzose dolostones and stromatolitic intervals. Throughout the basin, the top of the upper Sulky is marked by a prominent microbialite horizon, which contains and is interbedded with cauliflower chert and chert breccia, with the latter suggestive of evaporite dissolution and collapse. Shoaling of the September Lake reef complex into predominantly peritidal to supratidal deposits may reflect a fall in relative sea level, which ultimately led to evaporitic conditions and, possibly, exposure across much of the basin.

The overlying Greenhorn Formation is divided into two informal members (Kerans *et al*. 1981; Kerans, 1983; Kerans & Donaldson, 1988). The lower Greenhorn member consists of a monotonous sequence of microbially laminated dolostone in the east and rhythmically bedded shale and oolitic/stromatolitic dolostone in the west (Kerans *et al*. 1981), which record the re-establishment of peritidal conditions. The microbially laminated dolostone contains abundant chert, which preserves a variety of oscillatoriacean filamentous sheaths, entophysalidacean colonial coccoids, chroococcacean coccoids and the akinete *Archaeoellipsoides*. Such microfossil forms are common in the Dismal Lakes Group (Sulky and Greenhorn formations: Horodyski & Donaldson, 1980, 1983) and

are typical of Mesoproterozoic peritidal to supratidal successions (Hofmann & Jackson, 1991; Sergeev, 1994; Sergeev *et al*. 1994, Sergeev, Knoll & Grotzinger, 1995; Knoll & Sergeev, 1995). Oolites, stromatolite beds and intraformational breccias become increasingly common in the upper part of the lower Greenhorn member, suggesting the gradual development of high-energy conditions.

The contact between the lower and upper Greenhorn members is unconformable and marked by karst features, including sand- and flowstone-filled grikes, cave-floor stream deposits and collapse breccias up to 30 m thick (Kerans *et al*. 1981; Kerans, 1983; Kerans & Donaldson, 1988). Evidence for karsting becomes increasingly subtle to the west, where a thin lag of quartz arenite records post-karst deposition (Kerans & Donaldson, 1988). On the basis of stratigraphic relationships, Kerans (1983) suggested that lower Greenhorn deposition was terminated by the emplacement of the Muskox intrusion in the easternmost Coppermine Homocline, which resulted in > 60 m of tectonic uplift east of the Teshierpi Fault. The extent of palaeokarst development (from September Lake High to the Parry Bay-Kanuyak formations > 300 km to the east; Campbell, 1978; Kerans & Donaldson, 1988; Pelechaty *et al*. 1991) and the abundance of terrigenous material overlying the disconformity, however, suggest that uplift was of greater regional extent or, perhaps, coincident with a fall in sea level (Kerans & Donaldson, 1988). Strata of the upper Greenhorn are dominated by stromatolitic, oolitic and intraclastic dolostone, which record the re-establishment of the carbonate platform following subaerial exposure and karsting. Within the upper metres of the upper Greenhorn member, soft sediment deformation structures record interaction between wet sediment and hot lava, and indicate that carbonate deposition ended abruptly when flood basalts of the overlying Coppermine River Group were extruded across the basin (Kerans *et al*. 1981).

2.c. Age of the Dismal Lakes Group

The age of the Dismal Lakes Group is constrained by geochronological data derived from: (1) the underlying Narakay Volcanic Complex and (2) the Coppermine River Group, including flood basalts that cap the upper Greenhorn sequence. The Narakay Volcanic Complex, composed of marine strata and interbedded/cross-cutting bimodal volcanic rocks, represents the offshore equivalent of the upper Hornby Bay Group (Ross, 1982). Zircons from feldspar-phyric dykes and volcanic breccias associated with the final stage of felsic volcanism in the Narakay complex yield an age of 1662 ± 8 Ma (Bowring & Ross, 1985).

Although zircon data from the Narakay Volcanic Complex are useful in constraining the maximum age of the Dismal Lakes Group, identification of subsurface Coppermine Homocline strata west of the exposed outcrop belt, via drill cores (Aitken & Pugh, 1984) and seismic sections (Cook & Taylor, 1991; Cook & MacLean, 1992, 1995), suggest that the Hornby Bay–Dismal Lakes contact is regionally unconformable. Seismic interpretations (Cook & Taylor, 1991; Cook & MacLean, 1992) suggest that a period of compressional tectonism (Forward Orogeny: Cook & MacLean, 1995) led to regional block faulting and truncation of the Hornby Bay Group prior to the onset of Dismal Lakes deposition. Cook & MacLean (1995, 1996) related the Forward Orogeny to the Racklan Orogeny, which deformed similarly aged strata of the Wernecke Supergroup (Parrish & Bell, 1987) and the East Kootenay Orogeny (Anderson & Davis, 1995), which is believed to have terminated Belt Supergroup deposition at ~ 1370 Ma (Doughty & Chamberlain, 1996; Luepke & Lyons, 2001). These regional tectonic constraints indicate that the unconformity that caps the Hornby Bay Group records a significant period of time and suggest that deposition of the Dismal Lakes Group commenced sometime after 1370 Ma. Carbon isotope stratigraphy allows further revision of this estimate (see Section 4.d).

Cessation of Dismal Lakes deposition is marked by emplacement of the Muskox intrusion (Hoffman, 1980*b*; Kerans, 1983) and extrusion of the Coppermine River Group flood basalts over wet sediments of the Greenhorn Formation (Barager & Donaldson, 1973). The Muskox (1270 ± 4 Ma, U–$Pb_{baddelyite}$: LeCheminant & Heaman, 1989) is a layered ultramafic-to-mafic intrusion (Irvine, 1970) interpreted as the primary feeder chamber for flood basalts of the Coppermine River Group and associated dyke swarm. Combined, basalts of the Coppermine River Group and associated dykes are referred to as the Mackenzie igneous event and are dated at 1267 ± 2 Ma, U–$Pb_{baddelyite}$ (LeCheminant & Heaman, 1989).

3. Geochemical methods

Prior to sampling for geochemical analysis, polished slabs and thin-sections were examined using standard petrographic and cathodoluminescence microscopy to document the full range of textures and petrographic components. Samples (~ 2 mg) were drilled from polished slabs using hand-held and microscope-mounted drilling assemblies fitted with dental drill bits with tip diameters ranging from 20 to 1000 μm. These larger samples were split for paired stable isotopic and major element analyses; however, a number of smaller (50 to 100 μg) samples were collected in the same manner for stable isotopic analysis only.

Samples for stable carbon and oxygen isotope analysis (typically < 0.5 mg) were roasted under vacuum at 380 °C for one hour to remove volatile contaminants and were reacted with anhydrous phosphoric acid in individual reaction vessels of an on-line, automated MultiPrep device coupled to a VG Optima mass

spectrometer housed at Mountain Mass Spectrometry, Inc., Evergreen, Colorado, USA. Oxygen isotope ratios were corrected for ^{17}O contribution (Craig, 1957) and are reported in per mil (‰) relative to the VPDB (Vienna Pee Dee Belemnite) standard. Precision is better than 0.1 ‰ for $\delta^{13}C$ and $\delta^{18}O$ values and was monitored through daily analyses of NBS and other powdered calcite standards.

For determination of major element (Ca, Mg, Sr, Mn and Fe) concentrations, samples (0.5 to 2 mg) were digested in 2.5 ml of ultrapure 2N HNO_3. Solutions were then centrifuged, and 2.0 ml were pipetted to avoid insoluble residues. Measurements were performed at the University of Missouri using a Perkin Elmer Inductively Coupled Plasma Atomic Emission Spectrometer (ICP-AES) fitted with a microconcentric nebulizer and calibrated to a series of gravimetrically determined standards. Reproducibility, determined through replicate analysis of sample and standard solutions, is better than 5 % for Sr and Mn and better than 10 % for Ca, Mg and Fe.

4. Geochemical results

Geochemical data are provided in Tables 1 through 3. Petrographic components are plotted as three distinct groups in Figures 3, 4 and 5. These groups are: (1) microbially laminated dolostone, micrite and microspar, interpreted to have been deposited under subtidal to peritidal conditions; (2) primary precipitates (seafloor fans, microlaminated precipitates and microbialites with precipitated fabrics) and synsedimentary cements (herringbone cement and ooid/pisoid cortices); and (3) secondary cements, including those related to early (e.g. intergranular cement, cement in syneresis cracks and fenestrae/pore-filling cement) and late-stage diagenesis (e.g. blocky cement in void centres and cross-cutting fractures).

Carbon and oxygen isotope analyses reveal distinct differences in the composition of Group 3 components relative to those in Groups 1 and 2 (Fig. 3). Group 3 shows the lowest values of $\delta^{18}O$ (ranging to $<$–9 ‰) and $\delta^{13}C$ (–3.0 ‰ or lower for many samples). With oxygen isotope compositions between –4 ‰ and –7 ‰ and carbon isotope compositions ranging from –1.5 ‰ to +2.5 ‰, Group 1 and 2 components have higher and less-variable $\delta^{18}O$ and $\delta^{13}C$ values than recorded in the secondary cements that compose Group 3.

With the exception of some late-stage cement phases, the petrographic components are all largely dolomitized, with Mg/Ca ratios exceeding 0.5. Detailed fabric preservation in most depositional components and synsedimentary precipitates suggests that dolomitization occurred early in the diagenetic history of the Dismal Lakes Group, although secondary and tertiary diagenetic fabrics are also recognized. Strontium concentrations (Fig. 4, left) are typically $<$ 100 ppm, although higher concentrations occur in some Group 3 samples. Manganese concentrations are generally $< \sim$ 1000 ppm in Groups 1 and 2; higher concentrations, ranging to $\sim$ 4000 ppm, are observed in Group 3 (Fig. 4, right). All components are characterized by high Fe contents ($\sim$ 3000 ppm $\pm$ 200 for most components), reflecting the tendency of Fe^{2+} to substitute for Mg^{2+} and Ca^{2+} in the dolomite crystal structure (Tables 1–3).

4.a. Effects of diagenesis

When interpreting geochemical data from carbonate rocks, post-depositional effects must be considered. The effects of diagenesis, which may modify original isotopic and geochemical compositions, may be recognized through examination of elemental and isotopic trends (e.g. Veizer, 1983; Brand & Veizer, 1980; Choquette & James, 1990). Because of the disparity in relative concentrations of carbon and oxygen in water versus carbonate rock (oxygen concentrations are roughly equal, whereas carbon is concentrated in carbonate), exchange with meteoric or hydrothermal fluids tends to modify $\delta^{18}O$ values substantially before primary $\delta^{13}C$ values are affected (Lohmann, 1988; Banner & Hanson, 1990), although isotopic exchange with organic CO_2 may lead to slight ^{13}C depletion of carbonate (Valley, 1986). The coupled effects of these processes are typically expressed in carbonates that have undergone burial diagenesis as a covariant trend of sharply decreasing $\delta^{18}O$ with slightly decreasing $\delta^{13}C$ values (Choquette & James, 1990). Such a trend is evident in the Dismal Lakes data (Fig. 3), suggesting that original isotopic compositions have been modified to some degree. Most Group 1 and 2 components, however, have $\delta^{18}O$ values similar to those documented in other well-preserved Mesoproterozoic marine carbonates (e.g. Frank & Lyons, 2000; Kah, 2000), suggesting relatively little modification of primary signatures. By contrast, significantly lower $\delta^{18}O$ and $\delta^{13}C$ values in Group 3 components record diagenetic alteration. Furthermore, near the contact with the Coppermine Flood basalt, Group 1 and 2 components show significant depletions in ^{13}C and ^{18}O, suggesting that compositions were modified during interaction with hot fluids associated with lava eruption.

Although Mn/Sr ratios are useful indicators of diagenesis (Veizer, 1983), their application to understanding diagenesis is hampered by redox conditions during early diagenesis, which can promote relatively high Mn concentrations in pore fluids. The integrity of this ratio is also affected by Sr loss in carbonates that have undergone early dolomitization (Veizer, 1983; Carpenter *et al*. 1991). Despite these complications, the highest Mn^{2+} concentrations would be expected to occur in components affected by reducing pore waters during late-stage diagenesis (Choquette & James, 1990). Given these considerations, the observed pattern of higher Mn contents and lower $\delta^{18}O$ and $\delta^{13}C$ values

Table 1. Dismal Lakes Group isotopic and elemental compositions, September Lake (Measured Sections 1, 2, and 3)

Sample	Height (m)	Formation	Group	Phase	$\delta^{13}C$ (‰ VPDB)	$\delta^{18}O$ (‰ VPDB)	Mg/Ca	Sr (ppm)	Mn (ppm)	Fe (ppm)
Measured Section 1 (SL1)										
SL1-0-1	0	Kendall R.	1	micritic intraclast	0.0	−5.8	0.591	30	567	2730
SL1-0-2	0.0	Kendall R.	1	microspar	0.0	−5.0	0.638	31	433	2008
SL1-1-1	1.0	Kendall R.	1	microbial lamina	0.0	−5.5	0.619	32	469	2610
SL1-1-2	1.0	Kendall R.	1	microspar	−0.1	−4.9	0.604	30	458	1483
SL1-1-3	1.0	Kendall R.	3	void fill	−0.3	−7.1	0.615	21	741	4302
SL1-4	4.0	Kendall R.	2	synsedimentary precipitate	2.0	−5.0	0.614	32	560	2318
SL1-10	10.0	Sulky (l)	1	microspar	−0.6	−4.5	0.604	22	1155	6850
SL1-10	10.0	Sulky (l)	1	microspar	−0.6	−4.5	0.602	22	1150	6880
SL1-20	20.0	Sulky (l)	1	microspar	0.3	−5.2	0.601	23	663	7014
SL1-20	20.0	Sulky (l)	1	microspar	0.3	−5.2	0.599	26	682	7039
SL1-38	38.0	Sulky (l)	1	microspar	1.7	−4.3	0.670	30	319	3396
SL1-41	41.0	Sulky (m)	1	micrite	−0.2	−6.0	0.599	52	348	3302
SL1-50-1	50.0	Sulky (m)	2	synsedimentary precipitate	1.5	−3.2	0.637	57	179	1378
SL1-50-2	50.0	Sulky (m)	1	micrite	1.4	−4.0	0.603	51	311	2706
SL1-60	60.0	Sulky (m)	2	microbial precipitate	1.0	−4.3	0.583	37	543	3471
SL1-73-1	73.0	Sulky (m)	2	microbial precipitate	1.5	−3.5	0.633	40	217	1053
SL1-73-2	73.0	Sulky (m)	1	micrite	1.4	−6.4	0.603	31	912	4685
DS3-1.7-1	85.4	Sulky (u)	1	microspar	1.4	−5.8	0.566	31	226	1079
DS3-1.7-2	85.4	Sulky (u)	1	geopetal micrite	1.7	−5.0	0.619	36	262	1437
DS3-1.7-3	85.4	Sulky (u)	1	geopetal microspar	1.8	−4.0	0.579	42	230	1366
DS3-1.7-4	85.4	Sulky (u)	3	intergranular cement	1.0	−7.8	0.636	24	989	5597
DS3-1.7-5	85.4	Sulky (u)	3	intergranular cement	0.6	−10.9	0.529	21	1455	15080
DS3-1.7a-1	85.4	Sulky (u)	1	micrite	1.4	−6.0				
DS3-1.7a-2	85.4	Sulky (u)	2	synsedimentary precipitate	1.7	−4.1				
DS3-1.7a-3	85.4	Sulky (u)	2	synsedimentary precipitate	1.9	−4.2				
DS3-1.7a-4	85.4	Sulky (u)	3	intergranular cement	1.3	−6.4				
DS3-1.7a-5	85.4	Sulky (u)	3	intergranular cement	0.0	−8.0				
DS3-1.7a-6	85.4	Sulky (u)	2	synsedimentary precipitate	1.8	−4.4				
DS3-1.7a-7	85.4	Sulky (u)	2	pisoid cortex	1.8	−4.7				
DS3-1.7a-8	85.4	Sulky (u)	2	pisoid cortex	1.7	−4.8				
DS3-2.1-1	85.8	Sulky (u)	1	intragranular cement	1.7	−4.8	0.584	33	333	1754
DS3-2.1-2	85.8	Sulky (u)	1	micrite	1.7	−4.9	0.598	35	324	1897
DS3-2.1-3	85.8	Sulky (u)	3	void fill	1.2	−7.5	0.599	16	916	4371
DS3-2.1-4	85.8	Sulky (u)	3	void fill	−0.1	−9.3	0.546	34	3967	19739
DS3-2.1b-1	85.8	Sulky (u)	3	intergranular cement	0.9	−6.9				
DS3-2.1b-2	85.8	Sulky (u)	2	pisoid cortex	1.8	−4.9				
DS3-2.1b-3	85.8	Sulky (u)	2	pisoid cortex	1.8	−5.0				
DS3-3-1	86.7	Sulky (u)	1	micrite	1.8	−4.2	0.601	25	265	1386
DS3-3-2	86.7	Sulky (u)	1	micrite	1.8	−4.8				
DS3-3.8	87.5	Sulky (u)	1	microspar	1.7	−2.9	0.606	34	325	1630
DS3-10-1	93.7	Sulky (u)	1	microspar	1.6	−5.5	0.588	26	400	2331
DS3-10-2	93.7	Sulky (u)	3	void fill	1.5	−5.0	0.577	30	318	1513
DS3-10-3	93.7	Sulky (u)	1	micrite intraclast	1.5	−5.9	0.632	36	438	2917
DS3-19-1	102.7	Sulky (u)	1	micrite intraclast	1.6	−4.6	0.621	38	245	1415
DS3-19-2	102.7	Sulky (u)	1	microspar	1.2	−4.2	0.606	38	295	1507
DS3-20-1	103.7	Sulky (u)	1	micrite	1.5	−4.5	0.602	31	201	977
DS3-20-2	103.7	Sulky (u)	1	microspar	1.2	−4.0	0.600	28	203	1056
DS3-36-1	119.7	Sulky (u)	1	micrite	1.8	−4.9	0.580	28	271	1386
DS3-36-2	119.7	Sulky (u)	1	microspar	1.5	−5.3	0.584	36	437	2147
Measured Section 2 (SL2)										
S2-1-1	1.2	Sulky (l)	2	synsedimentary precipitate	−0.2	−5.3	0.640	32	792	2781
S2-1-2	1.2	Sulky (l)	3	fenestral cement	−0.2	−5.1	0.643	31	580	2062
S2-2	9.0	Sulky (l)	1	micrite	−0.3	−5.1	0.612	28	734	3606
S2-6	29.0	Sulky (l)	1	microspar	0.9	−5.9	0.593	27	875	8813
S2-56.5-1	36.5	Sulky (l)	2	microbial precipitate	1.5	−4.9	0.605	43	426	2766
S2-7	47.5	Sulky (l)	1	micrite	1.6	−5.5	0.615	39	1023	8291
S2-53	53.0	Sulky (m)	1	microbial micrite	1.6	−3.0	0.628	92	509	3939
S2-56.5-2	56.6	Sulky (m)	3	void fill	0.8	−8.9	0.583	20	1763	8858
ISM	56.8	Sulky (m)	1	micrite	1.4	−2.5				
ISM	56.8	Sulky (m)	1	micrite	1.4	−2.5	0.572	51	467	3125
LM	56.8	Sulky (m)	1	micrite	1.5	−2.8				
LM	56.8	Sulky (m)	1	micrite	1.4	−2.8	0.575	48	268	2177
ST	56.8	Sulky (m)	1	microbial microspar	1.2	−3.3	0.574	46	285	1904
ST	56.8	Sulky (m)	1	microbial microspar	1.2	−3.3				
S2-57	57.0	Sulky (m)	2	microbial precipitate	1.3	−3.7	0.601	55	265	1669
S2-67.5	67.5	Sulky (m)	2	microbial precipitate	1.5	−3.9	0.610	43	343	2070
S2-83	83.0	Sulky (m)	2	microbial precipitate	1.5	−4.2	0.599	34	411	1896
S2-95	95.0	Sulky (m)	2	microbial precipitate	1.5	−3.9	0.592	30	311	1487
SL2-1	134.0	Greenhorn (l)	1	micrite	1.7	−5.1	0.593	30	252	1194
SL2-5-1	138.0	Greenhorn (l)	1	micrite	1.7	−4.6	0.583	42	308	1335

Table 1 (*Cont.*)

Sample	Height (m)	Formation	Group	Phase	$\delta^{13}C$ (‰ VPDB)	$\delta^{18}O$ (‰ VPDB)	Mg/Ca	Sr (ppm)	Mn (ppm)	Fe (ppm)
SL2-5-1	138.0	Greenhorn (l)	1	micrite	1.7	−4.6	0.584	42	302	1301
SL2-5-2	138.0	Greenhorn (l)	3	void fill	0.0	−10.3	0.599	16	113	6173
SL2-9-1	142.0	Greenhorn (l)	1	micrite intraclast	−1.3	−4.8	0.607	42	319	1501
SL2-9-2	142.0	Greenhorn (l)	1	micrite	−1.7	−5.2	0.621	38	530	2924
SL2-21	154.0	Greenhorn (l)	2	synsedimentary precipitate	−1.1	−5.7	0.563	22	357	1714
SL2-23-1	156.0	Greenhorn (l)	3	intergranular cement	−0.9	−6.9				
SL2-23-2	156.0	Greenhorn (l)	3	intergranular cement	−1.1	−6.9				
SL2-23	156.0	Greenhorn (l)	1	micrite intraclast	−0.9	−5.0	0.600	26	427	1760
SL2-34-1	167.0	Greenhorn (l)	1	microspar	−0.8	−5.7	0.633	24	287	1102
SL2-34-2	167.0	Greenhorn (l)	3	void fill	−1.0	−7.5	0.571	23	938	3189
SL2-52-1	185.0	Greenhorn (u)	3	intergranular cement	−0.4	−7.9				
SL2-52-2	185.0	Greenhorn (u)	3	intergranular cement	−0.3	−6.4				
SL2-52-3	185.0	Greenhorn (u)	3	intergranular cement	−0.7	−6.7				
SL2-52-4	185.0	Greenhorn (u)	3	intergranular cement	−0.9	−6.0				
SL2-52	185.0	Greenhorn (u)	1	micrite intraclast	−0.1	−5.0	0.619	22	316	1464
SL2-62	195.0	Greenhorn (u)	2	synsedimentary precipitate	0.2	−5.3	0.630	33	249	1362
SL2-71	204.0	Greenhorn (u)	2	synsedimentary precipitate	0.2	−5.5	0.599	30	303	1478
SL2-71	204.0	Greenhorn (u)	2	synsedimentary precipitate	0.2	−5.5	0.598	30	306	1496
SL2-84	217.0	Greenhorn (u)	2	synsedimentary precipitate	0.4	−5.5	0.607	29	325	1690
SL2-94-1	227.0	Greenhorn (u)	2	synsedimentary precipitate	0.5	−5.1	0.599	47	270	1148
SL2-94-2	227.0	Greenhorn (u)	1	microspar	0.6	−5.7	0.610	30	319	1799
SL2-102-1	235.0	Greenhorn (u)	1	micrite	0.8	−5.4	0.598	24	499	1778
SL2-102b-1	235.0	Greenhorn (u)	1	micrite	0.5	−5.7				
SL2-102b-2	235.0	Greenhorn (u)	1	micrite	0.6	−5.3				
SL2-102-2	235.0	Greenhorn (u)	3	microbreccia	1.0	−5.8	0.602	30	291	1491
SL2-110	243.0	Greenhorn (u)	1	microspar	0.5	−5.6	0.562	31	359	1817
SL2-110	243.0	Greenhorn (u)	1	microspar	0.5	−5.6	0.559	31	350	1811
SL2-120	253.0	Greenhorn (u)	1	microbial micrite	−0.7	−6.7	0.554	67	1186	6663
SL2-124.5	257.5	Greenhorn (u)	1	micrite	1.1	−7.0	0.581	55	873	5922
SL2-125-1	258.0	Greenhorn (u)	1	microbial micrite	1.5	−7.3	0.589	55	835	6494
SL2-125b-1	258.0	Greenhorn (u)	1	micrite	1.7	−6.1				
SL2-125b-2	258.0	Greenhorn (u)	1	microbial micrite	1.5	−6.8				
SL2-125b-3	258.0	Greenhorn (u)	1	microbial micrite	1.5	−6.8				
SL2-125-2	258.0	Greenhorn (u)	1	microspar	−1.2	−6.9	0.605	62	537	5123
SL2-128	261.0	Greenhorn (u)	1	microspar	1.1	−7.6	0.566	61	612	4763
SL2-135	268.0	Greenhorn (u)	2	ooid	1.4	−5.2				
SL2-137	270.0	Greenhorn (u)	1	microbial microspar	1.2	−6.4	0.579	55	353	2165
SL2-137	270.0	Greenhorn (u)	1	microbial microspar	1.2	−6.4	0.579	55	358	2240
SL2-138	271.0	Greenhorn (u)	1	micrite	1.0	−4.7				
SL2-138	271.0	Greenhorn (u)	1	micrite	1.1	−4.4				
SL2-138	271.0	Greenhorn (u)	1	micrite intraclast	0.4	−6.2				
SL2-138	271.0	Greenhorn (u)	1	microspar	0.7	−6.1				
SL2-141	273.0	Greenhorn (u)	1	micrite	1.0	−6.2				
SL2-141	273.0	Greenhorn (u)	1	micrite	1.1	−5.6				
SL2-142	274.0	Greenhorn (u)	1	micrite	0.9	−6.9				
SL2-143	275.0	Greenhorn (u)	3	intergranular cement	0.6	−8.4				
SL2-144.5	276.5	Greenhorn (u)	1	micrite intraclast	0.7	−4.8				
SL2-146	278.0	Greenhorn (u)	1	micrite	−1.4	−10.2				
SL2-147.6	280.6	Greenhorn (u)	1	microbial microspar	0.5	−9.0				
SL2-150.7	282.7	Greenhorn (u)	1	micrite	−1.2	−7.6				
SL2-151.8	283.8	Greenhorn (u)	1	micrite	−0.9	−4.2				
SL2-151.8	283.8	Greenhorn (u)	2	ooid	0.4	−4.8				
SL2-153	286.0	Greenhorn (u)	1	microspar	−0.2	−6.6	0.606	310	356	2372
SL2-156.5	288.5	Greenhorn (u)	1	microspar	−1.8	−5.5				
SL2-156.5	288.5	Greenhorn (u)	1	microspar	−0.8	−5.0				
SL2-156.5	288.5	Greenhorn (u)	1	microspar	−0.1	−5.1				
SL2-158	290.0	Greenhorn (u)	1	micrite	−1.1	−6.4				
SL2-158	290.0	Greenhorn (u)	1	microbial micrite	−1.3	−7.4				
SL2-158	290.0	Greenhorn (u)	1	microspar	−1.7	−7.4				
SL2-158	290.0	Greenhorn (u)	1	microspar	−1.4	−7.1				
SL2-157.5-1	290.5	Greenhorn (u)	1	microbial microspar	−0.2	−7.2	0.591	151	223	2116
SL2-157.5-2	290.5	Greenhorn (u)	1	microspar	−0.7	−8.1	0.583	80	194	2240
SL2-172	305.0	Greenhorn (u)	1	microspar	0.3	−5.7	0.607	32	327	1850
SL2-176.5	308.5	Greenhorn (u)	3	intergranular cement	−2.6	−9.1				
SL2-176.5	308.5	Greenhorn (u)	3	intergranular cement	−2.2	−14.5				
SL2-178.9	310.9	Greenhorn (u)	3	intergranular cement	−2.8	−16.2				
SL2-178	311.0	Greenhorn (u)	1	micrite	−2.7	−13.7	0.563	72	120	942
SL2-178	311.0	Greenhorn (u)	1	micrite	−2.7	−13.7	0.566	72	122	937
Measured Section 3 (SLW)										
SLW-3	3.0	Sulky (m)	1	micrite	1.8	−5.9	0.572	23	702	7362
SLW-13	13.0	Sulky (m)	1	microspar	1.9	−6.0	0.570	22	354	4874

Table 1 (*Cont.*)

Sample	Height (m)	Formation	Group	Phase	$\delta^{13}C$ (‰ VPDB)	$\delta^{18}O$ (‰ VPDB)	Mg/Ca	Sr (ppm)	Mn (ppm)	Fe (ppm)
SLW-20	20.0	Sulky (m)	1	microspar	1.4	−4.9	0.584	20	586	6633
SLW-20	20.0	Sulky (m)	1	microspar	1.4	−4.9	0.586	20	589	6569
SLW-28	28.0	Sulky (m)	1	micrite	1.1	−4.8	0.578	24	549	4063
SLW-36	36.0	Sulky (m)	1	micrite	1.4	−3.2	0.564	54	883	4381
SLW-37-1	37.0	Sulky (m)	1	microspar	1.4	−4.2	0.564	30	226	1443
SLW-37-2	37.0	Sulky (m)	1	micrite	1.4	−3.1	0.561	36	169	1045
SLW-42	42.0	Sulky (m)	1	microspar	1.2	−3.9	0.563	41	376	3034
SLW-53-1	53.0	Sulky (m)	2	microbial precipitate	1.3	−3.9	0.530	37	419	2727
SLW-53-2	53.0	Sulky (m)	2	microbial precipitate	1.1	−3.8	0.518	38	379	1652
SLW-53-3	53.0	Sulky (m)	3	fenestral cement	0.9	−7.4	0.507	19	653	3781
SLW-60	60.0	Sulky (m)	1	microbial microspar	1.9	−3.8	0.579	38	354	2385
SLW-74	74.0	Sulky (m)	1	microspar	1.0	−5.9	0.583	41	323	2153
SLW-82	82.0	Sulky (u)	2	synsedimentary precipitate	1.6	−5.7	0.566	29	351	1657
SLW-82-1	82.0	Sulky (u)	3	void fill	1.7	−7.0				
SLW-82-2	82.0	Sulky (u)	3	intergranular cement	1.8	−4.6				
SLW-82-3	82.0	Sulky (u)	3	intergranular cement	0.8	−7.2				
SLW-82-4	82.0	Sulky (u)	2	pisoid cortex	1.7	−5.0				
SLW-82-5	82.0	Sulky (u)	2	pisoid cortex	1.9	−4.8				
SLW-82-6	82.0	Sulky (u)	2	pisoid cortex	1.7	−5.5				
SLW-90a	90.0	Sulky (u)	1	microbial microspar	1.9	−5.2	0.572	34	376	2059
SLW-90b-1	90.0	Sulky (u)	3	void fill	1.4	−12.8				
SLW-90b-2	90.0	Sulky (u)	3	void fill	1.6	−10.5				
SLW-90b-3	90.0	Sulky (u)	3	void fill	2.2	−5.7				
SLW-90b-4	90.0	Sulky (u)	2	pisoid cortex	2.0	−4.8				
SLW-99-1	99.0	Sulky (u)	3	intergranular cement	1.4	−10.1				
SLW-99-2	99.0	Sulky (u)	3	intergranular cement	1.8	−4.1				
SLW-99-3	99.0	Sulky (u)	3	intergranular cement	1.9	−3.9				
SLW-99-4	99.0	Sulky (u)	2	pisoid cortex	1.8	−4.4				
SLW-116-1	116.0	Greenhorn (l)	2	synsedimentary precipitate	−1.7	−6.4	0.526	29	657	3694
SLW-116-2	116.0	Greenhorn (l)	3	fenestral cement	−3.5	−9.7	0.599	25	643	3464
SLW-130	130.0	Greenhorn (l)	1	microspar	−1.0	−5.9	0.613	25	345	1670
SLW-137-1	137.0	Greenhorn (u)	1	microspar	−0.8	−5.4	0.617	26	278	1276
SLW-137-2	137.0	Greenhorn (u)	3	fenestral cement	−0.8	−6.9				
SLW-153	153.0	Greenhorn (u)	2	synsedimentary precipitate	−0.4	−5.2	0.576	30	273	1550
SLW-162	162.0	Greenhorn (u)	1	micrite	0.2	−5.8	0.574	25	647	2938
SLW-162	162.0	Greenhorn (u)	1	micrite	0.2	−5.8	0.569	26	648	3007
SLW-181	181.0	Greenhorn (u)	2	synsedimentary precipitate	−0.1	−7.0	0.582	27	299	1588
SLW-181-1	181.0	Greenhorn (u)	3	intergranular cement	0.3	−5.3				
SLW-181-2	181.0	Greenhorn (u)	1	microspar	0.3	−5.4				
SLW-190	190.0	Greenhorn (u)	3	bulk rock	0.5	−5.0	0.572	35	251	860
SLW-190	190.0	Greenhorn (u)	3	bulk rock	0.5	−5.0	0.572	34	258	879
SLW-201	201.0	Greenhorn (u)	1	micrite	0.5	−5.4	0.580	260	396	1863
SL3U-1	226.0	Greenhorn (u)	1	microbial microspar	0.5	−5.1	0.570	34	321	1419
SL3U-10	235.0	Greenhorn (u)	1	microspar	0.7	−6.1	0.552	26	311	1854
SL3U-23	248.0	Greenhorn (u)	1	microspar	0.4	−5.3	0.583	29	325	1643
SL3U-36.5-1	261.5	Greenhorn (u)	1	micrite	1.3	−6.2				
SL3U-36.5-1	261.5	Greenhorn (u)	1	micrite	1.5	−6.6				
SL3U-36.5-1	261.5	Greenhorn (u)	1	micrite	1.2	−7.7				
SL3U-38.5	263.5	Greenhorn (u)	1	microbial microspar	0.6	−7.8	0.569	52	433	6329
SL3U-42.5-1	267.5	Greenhorn (u)	1	micrite	−0.3	−6.3	0.558	59	238	996
SL3U-42.5-2	267.5	Greenhorn (u)	3	intergranular cement	−0.1	−10.4	0.574	1241	1113	5408
SL3U-52b	277.0	Greenhorn (u)	1	micrite	0.9	−8.3	0.563	44	773	3607
SL3U-52a	277.0	Greenhorn (u)	2	ooid	0.9	−8.4	0.567	45	792	3974
SL3U-52a-1	277.0	Greenhorn (u)	2	ooid	1.3	−8.5				
SL3U-52a-2	277.0	Greenhorn (u)	2	ooid	1.0	−7.6				
SL3U-52b-1	277.0	Greenhorn (u)	3	intergranular cement	1.1	−7.7				
SL3U-52b-2	277.0	Greenhorn (u)	3	intergranular cement	0.6	−10.7				
SL3U-52b-3	277.0	Greenhorn (u)	3	intergranular cement	1.1	−7.0				
SL3U-52b-4	277.0	Greenhorn (u)	3	intergranular cement	1.2	−7.8				
SL3U-59b-1	284.0	Greenhorn (u)	3	intergranular cement	0.8	−10.0				
SL3U-59b-2	284.0	Greenhorn (u)	3	intergranular cement	1.0	−6.8				
SL3U-59b-3	284.0	Greenhorn (u)	3	intergranular cement	0.7	−8.4				
SL3U-59a	284.0	Greenhorn (u)	3	microbreccia	0.9	−7.4	0.567	54	367	2834
SL3U-79.5	304.5	Greenhorn (u)	1	micrite	0.8	−4.4				
SL3U-79.5	304.5	Greenhorn (u)	1	micrite	0.8	−4.4				
SL3U-79.5	304.5	Greenhorn (u)	2	synsedimentary precipitate	0.4	−9.4				
SL3U-79.5	304.5	Greenhorn (u)	3	fenestral cement	0.4	−9.4				
SL3U-81	306.0	Greenhorn (u)	1	micrite	0.0	−3.8				
SL3U-81	306.0	Greenhorn (u)	1	micrite	0.0	−3.8				
SL3U-84	309.0	Greenhorn (u)	1	micrite	0.1	−3.7				
SL3U-84	309.0	Greenhorn (u)	1	micrite	0.1	−3.7				

Table 1 (*Cont.*)

Sample	Height (m)	Formation	Group	Phase	$\delta^{13}C$ (‰ VPDB)	$\delta^{18}O$ (‰ VPDB)	Mg/Ca	Sr (ppm)	Mn (ppm)	Fe (ppm)
SL3U-84.5	309.5	Greenhorn (u)	1	micrite	−0.2	−5.6				
SL3U-84.5	309.5	Greenhorn (u)	1	micrite	−1.3	−7.7				
SL3U-84.5	309.5	Greenhorn (u)	1	micrite	−1.3	−7.7				
SL3U-84.5	309.5	Greenhorn (u)	1	micrite	−0.2	−5.6				
SL3U-86.6	311.6	Greenhorn (u)	1	micrite	−1.2	−8.0				
SL3U-86.6	311.6	Greenhorn (u)	1	micrite	−1.2	−8.0				
SL3U-86.6	311.6	Greenhorn (u)	1	microspar	−0.5	−7.1				
SL3U-86.6	311.6	Greenhorn (u)	1	microspar	−0.5	−7.1				
SL3U-87	312.0	Greenhorn (u)	1	micrite	0.4	−4.1				
SL3U-87	312.0	Greenhorn (u)	1	micrite	1.2	−1.8				
SL3U-87	312.0	Greenhorn (u)	3	bulk rock	0.4	−4.1				
SL3U-87	312.0	Greenhorn (u)	3	bulk rock	1.2	−1.8				
SL3U-87.9	312.9	Greenhorn (u)	3	bulk rock	−2.8	−14.9				
SL3U-87.9	312.9	Greenhorn (u)	3	bulk rock	−2.7	−15.4				
SL3U-87.9	312.9	Greenhorn (u)	3	bulk rock	−2.7	−15.4				
SL3U-87.9	312.9	Greenhorn (u)	3	bulk rock	−2.8	−14.9				
SL3U-88.3	313.3	Greenhorn (u)	3	basalt vesicle fill	−1.9	−9.1				

Table 2. Dismal Lakes Group isotopic and elemental compositions, Dismal Lake (Measured Sections 4 and 5)

Sample	Height (m)	Formation	Group	Phase	$\delta^{13}C$ (‰ VPDB)	$\delta^{18}O$ (‰ VPDB)	Mg/Ca	Sr (ppm)	Mn (ppm)	Fe (ppm)
Measured Section 4 (DL1)										
DL1-3	3.0	Kendall R.	2	ooid	0.5	−6.1	0.547	24	808	4370
DL1-5.2-1	5.2	Kendall R.	1	micrite	0.7	−5.3	0.594	18	470	2894
DL1-5.2-2	5.2	Kendall R.	3	void fill	0.2	−12.7	0.512	44	4708	42669
DL1-5.2b-1	5.2	Kendall R.	2	ooid	0.8	−5.0				
DL1-5.2b-2	5.2	Kendall R.	2	ooid	0.8	−5.1				
DL1-5.2b-3	5.2	Kendall R.	2	ooid	0.9	−5.0				
DL1-7-2	7.0	Kendall R.	3	fracture fill	−1.0	−9.6				
DL1-7-1	7.0	Kendall R.	1	micrite	0.4	−6.1	0.591	19	653	4016
DL1-9-2	9.0	Kendall R.	1	micrite	0.6	−5.2	0.578	29	428	2020
DL1-9-3	9.0	Kendall R.	1	microspar	0.6	−4.9	0.581	30	374	1558
DL1-9-1	9.0	Kendall R.	2	synsedimentary precipitate	0.7	−5.4	0.581	26	592	3185
DL1-21	21.0	Kendall R.	3	microbreccia	0.3	−4.0	0.561	33	551	1754
DL1-31	31.0	Kendall R.	1	microspar	−0.4	−4.7	0.571	27	676	4663
DL1-42	42.0	Sulky (l)	1	micrite	1.2	−4.1	0.597	37	658	9058
DL1-43.5	43.5	Sulky (l)	1	micrite	0.2	−6.7	0.563	26	623	7290
DL1-48	48.0	Sulky (l)	1	micrite	0.8	−5.8	0.532	29	928	4641
DL1-48	48.0	Sulky (l)	1	micrite	0.8	−5.8	0.556	22	929	4696
DL1-48	48.0	Sulky (l)	1	micrite	0.8	−5.8	0.563	26	932	4735
DL1-59	59.0	Sulky (l)	1	micrite	1.5	−4.2	0.581	23	842	4423
DL1-67	67.0	Sulky (l)	1	micrite	1.6	−2.4	0.584	34	790	3147
DL1-76	76.0	Sulky (l)	1	micrite	1.3	−6.0	0.565	30	998	4583
DL1-76	76.0	Sulky (l)	1	micrite	1.3	−6.0	0.567	30	993	4620
DL1-88	88.0	Sulky (m)	2	microbial precipitate	1.7	−5.3	0.555	35	533	3449
DL1-88	88.0	Sulky (m)	2	microbial precipitate	1.7	−5.3	0.550	36	537	3493
DL1-159	159.0	Sulky (m)	1	micrite	2.0	−6.3	0.570	38	592	1985
DL1-168	168.0	Sulky (u)	1	microspar	2.1	−6.1	0.559	34	404	2188
DL1-186	186.0	Sulky (u)	3	bulk rock	2.3	−6.6	0.585	40	312	2357
DL1-186	186.0	Sulky (u)	3	bulk rock	2.3	−6.6	0.554	33	399	2139
DL1-201	201.0	Sulky (u)	1	microspar	2.1	−6.2	0.566	35	378	1867
DL1-214-1	214.0	Sulky (u)	1	microbial microspar	2.1	−5.5	0.590	26	213	1066
DL1-214-2	214.0	Sulky (u)	1	microspar	2.2	−4.7	0.570	33	154	896
DL1-214-2	214.0	Sulky (u)	1	microspar	2.2	−4.7	0.559	34	153	887
DL1-222	222.0	Sulky (u)	1	microspar	1.5	−6.3	0.576	29	412	1863
DL1-231	231.0	Sulky (u)	1	microspar	1.7	−4.1	0.562	44	285	1408
DL1-240	240.0	Sulky (u)	1	microspar	2.0	−6.1	0.579	23	368	1707
DL1-263-1	263.0	Greenhorn (l)	2	synsedimentary precipitate	−0.7	−5.4	0.534	29	237	1013
DL1-263-1	263.0	Greenhorn (l)	2	synsedimentary precipitate	−0.7	−5.4	0.566	32	242	1068
DL1-263-2	263.0	Greenhorn (l)	1	microspar	−0.7	−5.1	0.543	38	280	791
DL1-278	278.0	Greenhorn (l)	3	microbreccia	−0.3	−5.5	0.581	41	255	888
DL1-286-1	286.0	Greenhorn (l)	1	microspar	0.2	−5.4	0.585	35	277	1053
DL1-286-2	286.0	Greenhorn (l)	3	fracture fill	−1.2	−8.4	0.588	43	6516	5864
DL1-298	298.0	Greenhorn (l)	1	micrite	0.4	−6.1	0.587	31	375	1664
DL1-306-1	306.0	Greenhorn (l)	3	microbreccia	0.6	−5.3	0.567	39	314	1173
DL1-306-2	306.0	Greenhorn (l)	3	void fill	0.2	−11.6				
DL1-315	315.0	Greenhorn (l)	2	synsedimentary precipitate	0.9	−5.9	0.593	37	342	1222

Table 2 (*Cont.*)

Sample	Height (m)	Formation	Group	Phase	$\delta^{13}C$ (‰ VPDB)	$\delta^{18}O$ (‰ VPDB)	Mg/Ca	Sr (ppm)	Mn (ppm)	Fe (ppm)
DL1-318-1	318.0	Greenhorn (l)	1	microspar	1.0	−6.3	0.551	41	374	1713
DL1-318-2	318.0	Greenhorn (l)	2	synsedimentary cement	1.0	−5.2	0.620	46	268	798
DL1-324-2	324.0	Greenhorn (l)	3	fracture fill	0.7	−13.8				
DL1-324-1	324.0	Greenhorn (l)	2	microlaminated precipitates	1.1	−5.5	0.595	38	441	1248
DL1-324-1	324.0	Greenhorn (l)	2	microlaminated precipitates	1.1	−5.5	0.589	31	436	1216
DL1-324-1	324.0	Greenhorn (l)	2	microlaminated precipitates	1.1	−5.5	0.588	32	425	1207
DL1-332	332.0	Greenhorn (l)	1	microspar	1.1	−6.1	0.569	31	323	1669
DL1-341	341.0	Greenhorn (l)	1	microspar	1.0	−5.9	0.584	39	400	1630
DL1-351-1	351.0	Greenhorn (l)	1	microspar	1.5	−6.6	0.585	34	741	2936
DL1-351-2	351.0	Greenhorn (l)	2	synsedimentary cement	0.8	−6.7	0.565	27	653	2883
DL1-364-1	364.0	Greenhorn (l)	1	micrite	1.7	−5.2	0.588	38	438	2370
DL1-364-2	364.0	Greenhorn (l)	1	microspar	1.7	−5.0	0.578	36	432	2132
DL1-372-1	372.0	Greenhorn (l)	1	microspar	1.6	−6.1	0.576	34	397	2053
DL1-372-2	372.0	Greenhorn (u)	2	synsedimentary cement	1.7	−4.8	0.584	37	306	1035
DL1-397-1	397.0	Greenhorn (u)	1	microspar	1.4	−5.1	0.549	40	497	1961
DL1-397-2	397.0	Greenhorn (u)	2	synsedimentary cement	1.0	−5.6	0.614	43	464	1435
DL1-397-3	397.0	Greenhorn (u)	2	synsedimentary cement	0.8	−13.4	0.580	37	3335	7680
DL1-3T	460.0	Greenhorn (u)	1	micrite	2.0	−6.7	0.585	56	308	4567
DL1-11.9T-1	468.9	Greenhorn (u)	1	microbial micrite	1.1	−7.5	0.573	54	226	4600
DL1-11.9T-2	468.9	Greenhorn (u)	1	microspar	0.8	−8.2	0.570	50	220	3743
DL1-11.9T-A1	468.9	Greenhorn (u)	1	micrite intraclast	0.9	−6.9	0.576	88	233	4773
DL1-11.9T-A2	468.9	Greenhorn (u)	3	intergranular cement	0.9	−6.8	0.584	158	228	4989
DL1-11.9T-A3	468.9	Greenhorn (u)	2	microbreccia	0.7	−7.7	0.598	488	241	5716
DL1-11.9T-C1	468.9	Greenhorn (u)	1	microbial micrite	1.0	−8.0	0.574	111	236	5549
DL1-11.9T-C2	468.9	Greenhorn (u)	1	microspar	1.1	−8.1	0.581	75	221	4066
DL1-11.9T-C3	468.9	Greenhorn (u)	3	void fill	0.5	−9.9	0.625	9376	286	8629
DL1-17.9T-1	474.9	Greenhorn (u)	2	ooid	0.4	−11.5	0.583	65	244	5775
DL1-17.9T-2	474.9	Greenhorn (u)	1	micrite	0.4	−7.0	0.580	81	281	7154
DL1-17.9T-3	474.9	Greenhorn (u)	1	micrite	0.6	−7.1	0.579	72	241	6450
DL1-17.9T-4	474.9	Greenhorn (u)	3	microbreccia	0.6	−7.1	0.573	400	228	3458
DL1-17.9T-5	474.9	Greenhorn (u)	3	intergranular cement	0.6	−7.1	0.586	9482	288	8702
DL1-23.7T	480.7	Greenhorn (u)	1	micrite	1.6	−6.3	0.539	55	158	2137
DL1-28T-2	485.0	Greenhorn (u)	3	intergranular cement	1.1	−6.3				
DL1-28T-3	485.0	Greenhorn (u)	3	bulk rock	1.3	−6.4				
DL1-28T-4	485.0	Greenhorn (u)	1	micrite	1.4	−6.2				
DL1-28T	485.0	Greenhorn (u)	2	ooid	0.7	−8.0	0.542	86	286	2847
DL1-28T-1	485.0	Greenhorn (u)	2	ooid	0.9	−7.7				
DL1-28.8	485.8	Greenhorn (u)	2	ooid	1.5	−6.7	0.556	63	172	2662
DL1-28.8-1	485.8	Greenhorn (u)	2	ooid	1.4	−7.0				
DL1-33.7T	490.7	Greenhorn (u)	1	micrite	1.5	−7.5	0.571	70	155	1983
DL1-35.2T	492.2	Greenhorn (u)	2	synsedimentary precipitate	1.2	−7.6	0.531	53	168	1933
DL1-38T-1	495.0	Greenhorn (u)	1	micrite	2.0	−6.2	0.565	56	202	2382
DL1-38T-1	495.0	Greenhorn (u)	1	micrite	2.0	−6.2	0.566	61	198	2433
DL1-38T-2	495.0	Greenhorn (u)	3	microbreccia	1.7	−6.5	0.568	58	169	2743
DL1-39.9T	496.9	Greenhorn (u)	2	synsedimentary precipitate	1.7	−6.4	0.583	53	168	2037
DL1-42.5T	499.5	Greenhorn (u)	1	micrite	1.3	−6.1	0.565	50	190	1552
DL1-43T-1	500.0	Greenhorn (u)	1	micrite intraclast	0.4	−7.5				
DL1-43T-1	500.0	Greenhorn (u)	1	micrite intraclast	1.2	−5.0				
DL1-43T-1	500.0	Greenhorn (u)	1	microspar	1.0	−6.1				
DL1-47.9T	504.9	Greenhorn (u)	1	micrite	1.8	−6.8	0.536	43	483	2432
DL1-47.9T	504.9	Greenhorn (u)	1	micrite	1.8	−6.8	0.519	44	505	2522
DL1-50.5T	507.5	Greenhorn (u)	1	microspar	1.6	−7.3	0.590	41	493	2550
DL1-52T	509.0	Greenhorn (u)	1	microspar	1.4	−7.9				
DL1-54.2T	511.2	Greenhorn (u)	1	microspar	0.6	−7.5	0.589	39	1201	3626
Measured Section 5 (DL2)										
DL2-1	1.0	Kendall R.	3	microbreccia	0.7	−5.4	0.558	23	367	1989
DL2-2	2.0	Kendall R.	2	ooid	0.8	−4.9	0.557	20	304	2043
DL2-10-1	10.0	Kendall R.	2	ooid	0.9	−6.0				
DL2-10-2	10.0	Kendall R.	2	ooid	0.8	−6.1				
DL2-10-3	10.0	Kendall R.	3	intergranular cement	0.8	−6.2				
DL2-12-1	12.0	Kendall R.	3	bulk rock	0.8	−4.8				
DL2-12-2	12.0	Kendall R.	1	micrite	0.8	−4.7				
DL2-12-3	12.0	Kendall R.	3	intergranular cement	0.8	−4.8				
DL2-13-1	13.0	Kendall R.	1	micrite	0.5	−5.4	0.546	19	439	2527
DL2-13-2	13.0	Kendall R.	2	ooid	0.5	−5.5	0.567	17	414	3460
DL2-13a-1	13.0	Kendall R.	2	ooid	0.2	−5.6				
DL2-13a-2	13.0	Kendall R.	2	ooid	0.6	−4.9				
DL2-13a-3	13.0	Kendall R.	2	ooid	−0.2	−6.5				
DL2-19-1	19.0	Kendall R.	2	microlaminated precpitate	0.8	−4.7	0.623	0	404	1816
DL2-19-2	19.0	Kendall R.	1	microspar	0.7	−4.3	0.601	28	458	1181
DL2-28	28.0	Kendall R.	3	microbreccia	−0.6	−4.5	0.588	22	413	1546

Table 2 (*Cont.*)

Sample	Height (m)	Formation	Group	Phase	$\delta^{13}C$ (‰ VPDB)	$\delta^{18}O$ (‰ VPDB)	Mg/Ca	Sr (ppm)	Mn (ppm)	Fe (ppm)
DL2-36	36.0	Kendall R.	1	microspar	−0.1	−4.7	0.571	20	478	1808
DL2-43	43.0	Kendall R.	1	microspar	−0.8	−4.5	0.563	23	825	3843
DL2-43	43.0	Kendall R.	1	microspar	−0.8	−4.5	0.557	23	824	3814
DL2-64	64.0	Sulky (l)	1	micrite	1.5	−4.9	0.565	21	719	3601
DL2-95	95.0	Sulky (l)	1	micrite	1.8	−6.6	0.536	34	237	1563
DL2-102	102.0	Sulky (m)	2	synsedimentary precipitate	1.5	−6.8	0.575	33	294	1658
DL2-106	106.0	Sulky (m)	1	microspar	2.5	−6.3	0.566	25	367	2024
DL2-115	115.0	Sulky (m)	1	microspar	2.2	−6.7	0.595	24	349	1802
DL2-118	118.0	Sulky (m)	1	microspar	2.4	−6.5	0.579	23	437	2375
DL2-125	125.0	Sulky (m)	1	micrite	2.2	−7.1	0.565	31	537	3222
DL2-125	125.0	Sulky (m)	1	micrite	2.2	−7.1	0.562	32	531	3149
DL2-140	140.0	Sulky (m)	1	microspar	2.2	−7.0	0.576	30	727	3495
DL2-154	154.0	Sulky (m)	1	microspar	2.1	−7.5	0.545	32	707	2917
DL2-154	154.0	Sulky (m)	1	microspar	2.1	−7.5	0.543	31	716	2920
DL2-163	163.0	Sulky (m)	3	intergranular cement	2.2	−5.3	0.573	30	356	1605
DL2-174	174.0	Sulky (u)	1	microspar	2.1	−5.7	0.543	27	379	2115
DL2-183	183.0	Sulky (u)	2	synsedimentary precipitate	1.9	−7.0	0.586	33	393	1956
DL2-193-1	193.0	Sulky (u)	2	synsedimentary precipitate	1.6	−7.2	0.562	36	352	1385
DL2-193-1	193.0	Sulky (u)	2	synsedimentary precipitate	1.6	−7.2	0.562	36	348	1389
DL2-193-2	193.0	Sulky (u)	3	intergranular cement	1.0	−8.7	0.580	26	866	5622
DL2-202	202.0	Sulky (u)	1	micrite	2.0	−5.4	0.555	26	376	1529
DL2-213	213.0	Sulky (u)	1	microbial microspar	2.3	−5.0	0.598	20	284	1055
DL2-220-1	220.0	Sulky (u)	1	microbial microspar	1.7	−5.8	0.577	24	431	1343
DL2-220-2	220.0	Sulky (u)	1	micrite	1.8	−4.7	0.582	24	216	773
DL2-220a-1	220.0	Sulky (u)	1	micrite	1.7	−4.7				
DL2-220a-2	220.0	Sulky (u)	1	micrite	1.7	−4.8				
DL2-231	231.0	Sulky (u)	1	micrite	1.5	−5.0	0.578	22	215	879
DL2-235	235.0	Sulky (u)	2	ooid	0.0	−8.1	0.547	20	432	1443
DL2-235-1	235.0	Sulky (u)	2	ooid	1.7	−4.4				
DL2-235-2	235.0	Sulky (u)	2	ooid	1.3	−5.2				
DL2-242	242.0	Sulky (u)	3	microbreccia	2.0	−4.8	0.544	62	255	1265
DL2-253-1	253.0	Greenhorn (l)	1	micrite	−1.1	−5.4				
DL2-253-2	253.0	Greenhorn (l)	1	micrite	−1.2	−5.2				
DL2-270	270.0	Greenhorn (l)	1	microbial microspar	−0.9	−5.5	0.579	30	421	1715
DL2-281-1	281.0	Greenhorn (l)	1	micrite	−1.6	−5.4	0.561	31	447	1352
DL2-281-2	281.0	Greenhorn (l)	3	fracture fill	−0.6	−12.0	0.571	32	5249	12902
DL2-291	291.0	Greenhorn (l)	2	synsedimentary precipitate	−1.2	−5.2	0.587	26	428	1261
DL2-302	302.0	Greenhorn (l)	2	synsedimentary precipitate	−0.9	−5.8	0.580	28	294	1247
DL2-312-1	312.0	Greenhorn (l)	1	micrite	−0.3	−5.2	0.560	26	292	1130
DL2-312-1	312.0	Greenhorn (l)	1	micrite	−0.3	−5.2	0.561	25	293	1121
DL2-312-2	312.0	Greenhorn (l)	2	synsedimentary precipitate	−1.1	−6.9	0.556	26	390	1623
DL2-312b-1	312.0	Greenhorn (l)	3	intergranular cement	−0.3	−9.7				
DL2-312b-2	312.0	Greenhorn (l)	3	intergranular cement	−0.2	−9.7				
DL2-312b-3	312.0	Greenhorn (l)	3	intergranular cement	−0.3	−9.7				
DL2-312b-4	312.0	Greenhorn (l)	1	micrite intraclast	−0.7	−5.9				
DL2-327-1	327.0	Greenhorn (l)	1	microspar	0.3	−5.3	0.581	24	333	1120
DL2-327-2	327.0	Greenhorn (l)	3	fracture fill	−1.1	−9.4	0.523	28	7708	20027
DL2-327-3	327.0	Greenhorn (l)	3	fracture fill	−0.6	−11.7	0.593	28	4695	12519
DL2-335-1	335.0	Greenhorn (l)	1	microspar	0.1	−5.5	0.583	23	253	1049
DL2-335-2	335.0	Greenhorn (l)	3	fracture fill	−1.0	−8.3	0.527	28	9795	17377
DL2-345-1	345.0	Greenhorn (l)	1	micrite	0.1	−5.4	0.575	37	342	1546
DL2-345-2	345.0	Greenhorn (l)	3	void fill	0.1	−6.3	0.598	31	448	3059
DL2-355-1	355.0	Greenhorn (l)	1	micrite	0.4	−6.0	0.559	27	519	2503
DL2-355-2	355.0	Greenhorn (l)	1	microspar	0.3	−6.0	0.599	30	546	2457
DL2-371-1	371.0	Greenhorn (l)	3	microbreccia	0.6	−6.0	0.575	28	441	1819
DL2-371-1	371.0	Greenhorn (l)	3	microbreccia	0.6	−6.0	0.568	29	444	1834
DL2-371-2	371.0	Greenhorn (l)	3	void fill	0.4	−7.0	0.587	22	424	1740
DL2-371-3	371.0	Greenhorn (l)	3	void fill	0.2	−13.9	0.539	25	9917	8097
DL2-384	384.0	Greenhorn (l)	2	microlaminated precipitate	0.6	−5.8	0.580	34	389	1440
DL2-408	408.0	Greenhorn (l)	1	micrite intraclast	1.4	−5.5	0.578	18	601	2156
DL2-419-1	419.0	Greenhorn (l)	1	microspar	1.5	−5.8	0.569	25	1039	3008
DL2-419-2	419.0	Greenhorn (l)	3	fracture fill	0.9	−12.2	0.562	27	5306	8649

in Group 3 and, in contrast, lower Mn contents coupled with higher $\delta^{18}O$ and $\delta^{13}C$ values in Groups 1 and 2 is consistent with conclusions drawn on the basis of isotopic data alone.

In summary, trends in geochemical and isotopic data suggest that most Dismal Lakes carbonates record primary marine carbon isotope compositions. Notable exceptions are late-stage components (that is, ferroan dolomite cement in deep-water microbialites) and the uppermost part of the stratigraphic section, adjacent to the contact with the Coppermine River flood basalts. Retention of marine $\delta^{13}C$ values in these and other

Table 3. Isotopic and elemental compositions, basinal coniform microbialites (Measured Section 4)

Sample	Height (m)	Formation	Group	Phase	$\delta^{13}C$ (‰ VPDB)	$\delta^{18}O$ (‰ VPDB)	Mg/Ca	Sr (ppm)	Mn (ppm)	Fe (ppm)
PR-4.5-1	96.2	Sulky (m)	1	microbial microspar	1.6	−6.6	0.601	11	351	2876
PR-4.5-2	96.2	Sulky (m)	2	herringbone cement	1.5	−6.1	0.601	31	350	2220
PR-4.5-3	96.2	Sulky (m)	3	void fill	0.6	−14.9	0.579	29	4756	16148
PR-6-1	97.7	Sulky (m)	1	microbial microspar	1.5	−7.0	0.600	29	532	3494
PR-6-2	97.7	Sulky (m)	2	herringbone cement	1.8	−5.9	0.606	27	264	1455
PR-6-3	97.7	Sulky (m)	3	void fill	−0.6	−12.8	0.575	21	3843	12764
DL1-98-1	98.0	Sulky (m)	1	microbial microspar	1.8	−6.3	0.591	16	362	2873
DL1-98-2	98.0	Sulky (m)	2	herringbone cement	2.0	−6.0	0.608	34	289	1923
DL1-98-3	98.0	Sulky (m)	3	void fill	1.7	−8.6	0.604	20	456	3710
DL1-102-1	102.0	Sulky (m)	1	microbial microspar	1.8	−6.8	0.583	18	375	2754
DL1-102-2	102.0	Sulky (m)	2	herringbone cement	2.0	−5.3	0.606	35	229	1645
DL1-102-3	102.0	Sulky (m)	3	void fill	1.0	−14.4	0.549	27	3403	10074
DL1-102F-1	102.0	Sulky (m)	1	microbial microspar	1.8	−6.5	0.601	12	325	2145
DL1-102F-2	102.0	Sulky (m)	2	herringbone cement	1.7	−6.3	0.604	30	301	2020
DL1-102F-3	102.0	Sulky (m)	3	void fill	1.5	−14.4	0.582	40	4269	15246
PR-10.5A-1	102.2	Sulky (m)	1	microbial microspar	1.5	−7.3	0.596	32	423	2958
PR-10.5A-1	102.2	Sulky (m)	1	microbial microspar	1.5	−7.3	0.596	32	423	2958
PR-10.5A-2	102.2	Sulky (m)	2	herringbone cement	1.9	−6.6	0.597	33	246	1712
PR-10.5A-3	102.2	Sulky (m)	3	void fill	1.3	−13.1	0.587	23	2469	9275
PR-10.5B-2	102.2	Sulky (m)	2	herringbone cement	2.0	−6.3	0.606	30	248	1657
PR-10.5B-3	102.2	Sulky (m)	3	void fill	0.0	−12.7	0.582	25	3514	12156
DL1-103-1	103.0	Sulky (m)	1	microbial microspar	1.7	−7.1	0.598	11	258	2658
DL1-103-2	103.0	Sulky (m)	2	herringbone cement	2.0	−11.0	0.595	31	205	1622
DL1-103-2	103.0	Sulky (m)	2	herringbone cement	1.7	−10.8	0.606	34	205	1667
PR-12-1	103.7	Sulky (m)	1	microbial microspar	1.8	−7.3	0.600	28	537	4125
PR-12-2	103.7	Sulky (m)	2	herringbone cement	2.0	−5.8	0.608	32	191	1291
PR-12-3	103.7	Sulky (m)	3	void fill	1.4	−13.7	0.579	32	3145	12693
PR-12-3	104.0	Sulky (m)	3	void fill	1.4	−13.7	0.568	29	3056	12245
PR-19.5-1	111.2	Sulky (m)	1	microbial microspar	1.7	−6.1	0.601	31	349	1832
PR-19.5-2	111.2	Sulky (m)	2	herringbone cement	1.8	−6.3	0.605	30	414	1633
PR-19.5-3	111.2	Sulky (m)	3	void fill	0.6	−11.4	0.581	17	1522	7078
DL1-118-1	118.0	Sulky (m)	1	microbial microspar	1.8	−6.5	0.596	11	538	2496
DL1-118-2	118.0	Sulky (m)	2	herringbone cement	1.7	−6.2	0.614	31	523	2278
DL1-118-3	118.0	Sulky (m)	3	void fill	1.4	−10.4	0.563	20	1952	4191
DL1-128A-1	128.0	Sulky (m)	1	microbial microspar	2.0	−7.1	0.596	27	397	3376
DL1-128A-1	128.0	Sulky (m)	1	microbial microspar	2.0	−7.1	0.593	12	386	3244
DL1-128A-2	128.0	Sulky (m)	2	herringbone cement	2.1	−5.9	0.597	33	259	1819
DL1-128A-3	128.0	Sulky (m)	3	void fill	0.1	−14.4	0.362	25	3394	9797
DL1-128B-1	128.0	Sulky (m)	1	microbial microspar	1.8	−5.7	0.592	16	294	1768
DL1-128B-2	128.0	Sulky (m)	2	herringbone cement	1.82	−6.34	0.561	29	291	1650
DL1-128B-3	128.0	Sulky (m)	3	void fill	1.7	−9.3	0.604	17	369	3297
DL1-147-1	147.0	Sulky (m)	1	microbial microspar	1.7	−6.3	0.596	14	499	2640
DL1-147-2	147.0	Sulky (m)	2	herringbone cement	1.0	−10.2	0.593	25	309	1490
DL1-147-3	147.0	Sulky (m)	3	void fill	1.4	−12.3	0.590	21	2323	6571

Precambrian carbonates is favoured by factors that promote rock-dominated conditions during diagenetic alteration (low water–rock ratios), widespread syndepositional lithification and rapid stabilization of marine carbonate phases by early diagenetic, seawater-driven dolomitization (Knoll & Swett, 1990; Kaufman *et al*. 1991; Kah, 2000). Such conditions promote buffering of the $\delta^{13}C$ values of diagenetic fluids to host rock (primary marine) values, allowing for the retention of primary isotopic signatures in diagenetically altered carbonate phases.

4.b. Stratigraphic trends

Although there is considerable overall variation in $\delta^{13}C$, examination of data in a stratigraphic context reveals that most of the variation occurs as systematic, vertical trends (Fig. 5). Most carbonate strata of the upper Kendall River Formation (base of Sections 1, 4 and 5) have $\delta^{13}C$ values of 0–1 ‰; $\delta^{13}C$ values decrease slightly (by 0.5 ‰) upward toward the contact with the overlying Sulky Formation. Values increase gradually through the lower Sulky Formation, reaching a maximum (1.5 ‰ in Sections 1–3, and 2 ‰ in Sections 4 and 5) near the base of the middle Sulky Formation. The $\delta^{13}C$ values then remain relatively uniform to the base of the chert breccia, which forms the top of the upper Sulky Formation. Immediately above the chert breccia, $\delta^{13}C$ values drop to ∼–2 ‰ in Sections 2 and 3 and ∼–1 ‰ in Sections 4 and 5, above which they increase monotonically upward through the Greenhorn Formation toward the base of the Coppermine River flood basalts, which cap the sequence. The only exceptions to these trends are either (1) associated with samples that record interaction with late-stage diagenetic fluids, namely purple ferroan dolomites in deep-water cuspate microbialites (∼95–150 m, Section 4) and intergranular cements (base of

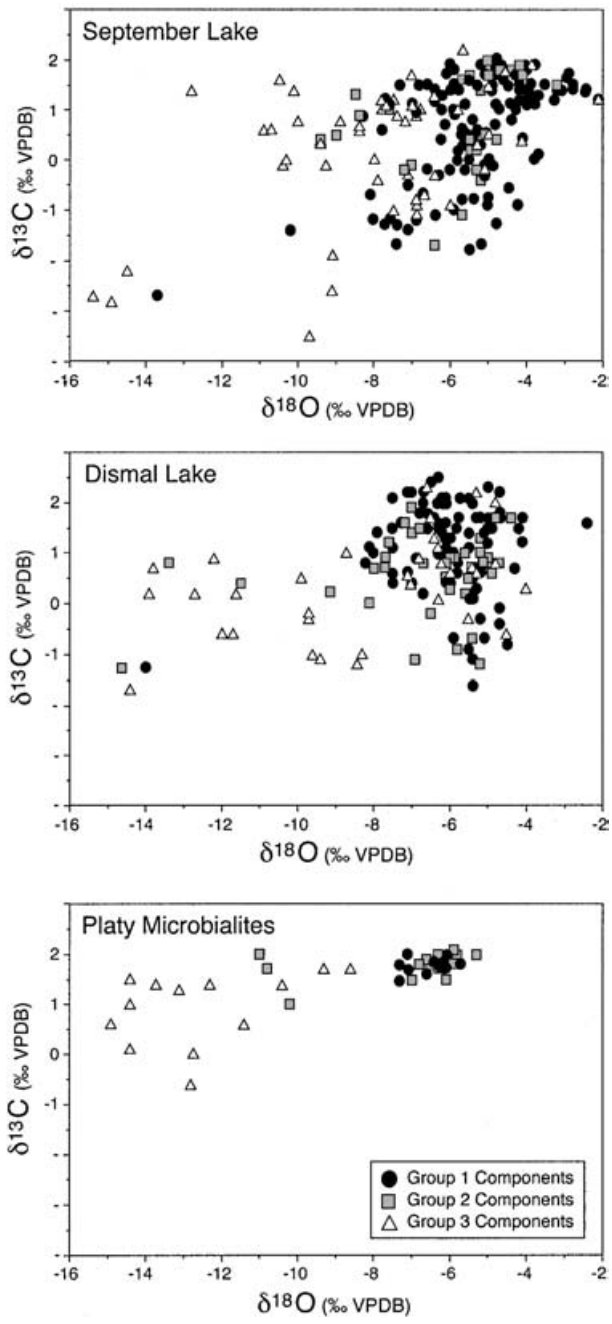

Figure 3. Carbon and oxygen isotope compositions from September Lake Sections 1–3 (top), Dismal Lake Sections 4–5 (middle) and Platy Microbialites at Section 4 (bottom). Symbols indicate petrographic components belonging to Group 1 (micritic and microsparitic components), Group 2 (synsedimentary precipitates) and Group 3 (secondary cements).

upper Sulky member, Section 1) or (2) samples from strata affected by extrusion of the Coppermine River flood basalts (tops of Sections 2 and 3).

The smooth and time-correlative nature of the $\delta^{13}C$ shifts in Dismal Lakes strata is consistent with changes expected to record secular variation in marine composition and favours a primary rather than diagenetic cause for vertical changes in $\delta^{13}C$ values (e.g. regional diagenesis of discrete stratigraphic intervals). The abrupt drop in $\delta^{13}C$ recorded across the chert breccia that marks a sequence boundary between the upper Sulky member and the Greenhorn Formation is interpreted to reflect nondeposition along a regional unconformity.

4.c. Basin-scale trends

Lateral variations in depositional environment are reflected in isotopic data as differences in the magnitude of $\delta^{13}C$ along stratigraphic horizons. The $\delta^{13}C$ values recorded in deeper water facies west of the Teshierpi Fault tend to be 0.5–1.0 ‰ higher than those recorded to the east of the fault within shallower water facies of the same stratigraphic interval (Fig. 5). These isotopic differences are most pronounced in the Greenhorn Formation. Higher rates of subsidence to the west resulted in the development of deeper water environments and/or less restricted water movement in western regions. Minor ^{13}C depletions in shallower/more restricted depositional settings have been observed in other Proterozoic dolostone successions, even where regional chemostratigraphic trends are similar. For example, lower $\delta^{13}C$ values are particularly common in laminated microbialites, where ^{13}C depletions on the order of ~ 1 ‰ have been recorded (e.g. Ghazban, Schwartz & Ford, 1992; Kah *et al*. 1999*a*). Petrographic observations (Kah & Knoll, 1996) suggest that lower $\delta^{13}C$ values in laminated microbial facies reflect *in situ* carbonate precipitation (within cyanobacterial mats) in the presence of isotopically light carbon released during the microbial degradation of organic matter. By contrast, $\delta^{13}C$ values of carbonate precipitated directly from the water column (ooids, sea floor precipitates and micrite forming in surface waters and settling to the sea floor) more accurately reflect the isotopic composition of marine water. Lateral facies variations in the Greenhorn Formation, marked by an increase in laminated microbialites from west to east, are consistent with this interpretation.

4.d. Comparison with older and younger records

Mesoproterozoic marine successions preserve a global transition in the marine $\delta^{13}C$ record from relatively static $\delta^{13}C$ values near 0 ‰ to values near +3.5 ‰ (Kah *et al*. 1999*a*). Although geochronological data constrain the timing of this isotopic transition to between ~ 1300 Ma and ~ 1200 Ma (Kah *et al*. 1999*a*; Bartley *et al*. 2001), the isotopic record between 1300 and 1200 Ma is not well understood. Carbon isotope compositions from the Allamoore Formation (1250^{+16}_{-24} Ma; Roths, 1993) range between +2 and +4 ‰ (Kah & Bartley, 1997), suggesting that carbon isotope compositions typical of the late Mesoproterozoic had been attained by ~ 1250 Ma. The carbon isotope record from the Dismal Lakes Group is characterized by $\delta^{13}C$ values that are generally higher and

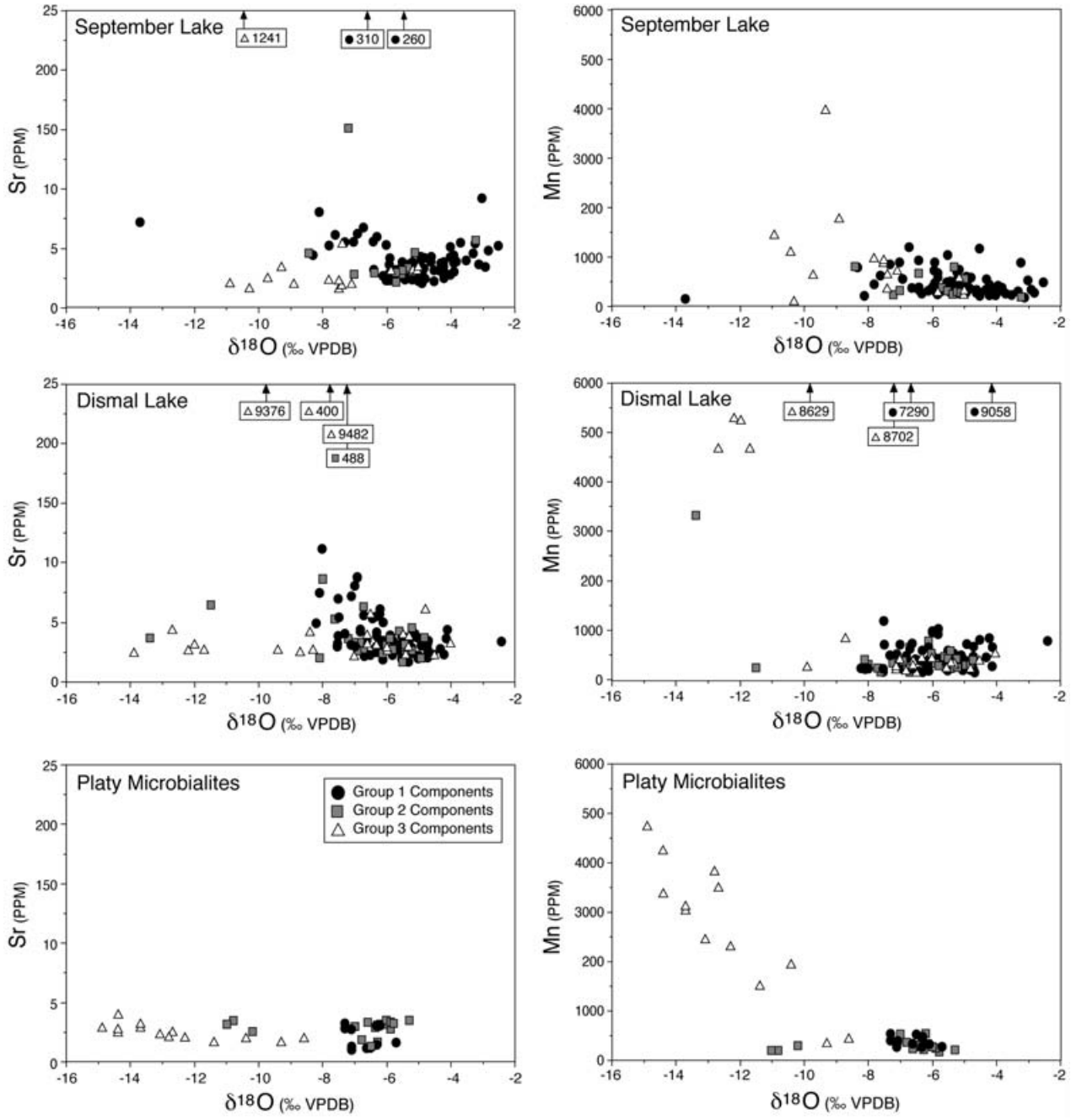

Figure 4. δ^{18}O values plotted v. Sr (left) and Mn (right) concentrations for samples from September Lake Sections 1–3 (top), Dismal Lake Sections 4–5 (middle) and Platy Microbialites at Section 4 (bottom). Symbols indicate petrographic components belonging to Group 1 (micritic and microsparitic components), Group 2 (synsedimentary precipitates) and Group 3 (secondary cements).

more variable than those typical of strata > 1300 Ma and, at the same time, lower and less variable than those typical of records younger than ~1250 Ma. Considered as a whole, chemostratigraphic data and the minimum age provided from the overlying Coppermine River Group (~1270 Ma) suggest that Dismal Lakes deposition commenced after 1300 Ma.

As data from the present study resolve the timing of the carbon isotope shift, it becomes apparent that as average δ^{13}C values increase, the lowest δ^{13}C values associated with negative excursions become increasingly more negative, resulting in an overall increase in the degree of isotopic variation with time. Isotopic excursions are relatively rare in late Palaeoproterozoic and early Mesoproterozoic (prior to ~1300 Ma) records, with minimum values rarely lower than ~–1.0‰ (cf. Buick, Des Marais & Knoll, 1995; Xiao *et al*. 1997; Frank, Lyons & Lohmann, 1997; Lindsay & Brasier, 2000). Late Mesoproterozoic marine carbonate successions, however, commonly show short-lived excursions to δ^{13}C values of ~–2‰ (this study; Fairchild, Marshall & Betrand-Sarfati,

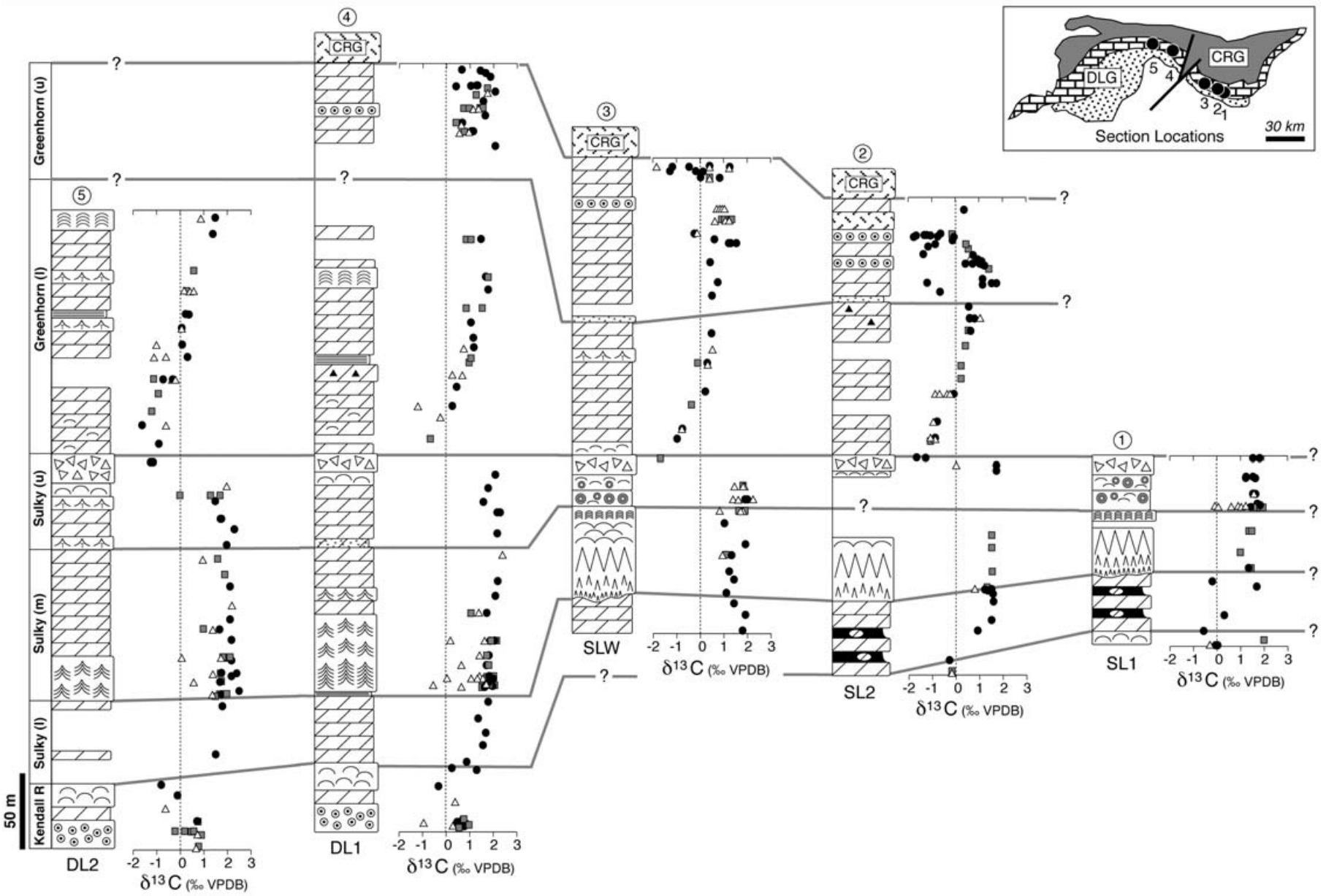

Figure 5. Stratigraphic and chemostratigraphic profiles from Dismal Lakes Group Sections 1 through 5. Inset map shows locality of measured sections, and symbols indicate petrographic components belonging to Group 1 (micritic and microsparitic components), Group 2 (synsedimentary precipitates) and Group 3 (secondary cements). For legends see Figures 2 and 3.

1990; Knoll, Kaufman & Semikhatov, 1995; Kah *et al*. 1999*a*; Bartley *et al*. 2001). Neoproterozoic records show short-lived negative excursions to $\delta^{13}C$ values of –2 ‰ to –4 ‰ (Kaufman & Knoll, 1995; Brasier *et al*. 1996; Kennedy, 1996; Kaufmann, Knoll & Narbonne, 1997; Hoffman, Kaufman & Halverson, 1998) and –6 ‰ or lower in the Vendian (Lambert *et al*. 1987; Magaritz *et al*. 1991; Narbonne, Kaufman & Knoll, 1994; Brasier *et al*. 1996; Kaufman *et al*. 1996; Pelechaty, Kaufman & Grotzinger, 1996; Bartley *et al*. 1998).

5. Discussion

Variation in marine $\delta^{13}C$ reflects changes in the ratio of organic C (C_{org}) to inorganic C (C_{carb}) that is removed from the oceans through burial of organic matter and sedimentary carbonate (Holland, 1984). Long-term excursions to higher marine $\delta^{13}C$ values reflect an increase in the removal of isotopically light organic carbon relative to carbonate carbon, whereas excursions to lower $\delta^{13}C$ values indicate the opposite. Preferential removal of C_{org} may be driven by a number of mechanisms, including increased biological productivity in surface waters leading to greater C_{org} burial, enhanced preservation of organic matter under anoxic conditions, and/or increased sedimentation rates associated with tectonic uplift (Demaison & Moore, 1980; Canfield, 1989, 1994). Assuming steady state conditions, these relationships may be expressed as

$$f_{org} = \frac{(\delta^{13}C_w - \delta^{13}C_{carb})}{\Delta_B}$$

where f_{org} represents the organic fraction of the total carbon burial flux, $\delta^{13}C_w$ represents the isotopic composition of carbon derived from the weathering and volcanic fluxes, $\delta^{13}C_{carb}$ is the composition of marine carbonate, and Δ_B is the isotopic difference between the C_{org} and C_{carb} removed from the ocean reservoir, expressed as a negative number (Holland, 1984). The above equation demonstrates that if Δ_B and $\delta^{13}C_w$ are constant, a change in the removal rate of C_{org} from the ocean system will be recorded in $\delta^{13}C_{carb}$ (Kump & Arthur, 1999).

Using the Mesoproterozoic record as an example, and specifying that $\Delta_B = -30$ ‰ (Des Marais, 1997) and $\delta^{13}C_w = -5$ ‰ (composition of the modern weathering flux), the observed isotopic shift in $\delta^{13}C_{carb}$ from 0 to +3.5 ‰ could be interpreted to reflect a 59 % increase in f_{org}, from 0.17 to 0.28. Des Marais *et al*. (1992) showed a similar increase (54 %) through this interval based on a compilation of data from Proterozoic sedimentary organic carbon and carbonate by Strauss *et al*. (1992). Assuming C_{org} fluxes in the ocean remained constant through this time, the observed mid-Mesoproterozoic isotopic shift would require a > 50 % increase in the burial preservation of C_{org}. In light of the relationships between marine $\delta^{13}C$ and f_{org}, increases in $\delta^{13}C_{carb}$ are often linked to high sedimentation rates during periods of mountain building, which is believed to promote burial preservation of C_{org} (e.g. Knoll, Kaufman & Semikhatov, 1986; Kaufman, Jacobsen & Knoll, 1993; Karhu & Holland, 1996; Des Marais, 1997). The Mesoproterozoic record, which shows a permanent shift in the marine $\delta^{13}C$ baseline, requires that elevated sedimentation rates were maintained for roughly 450 Ma (~ 1300–850 Ma) to sustain enhanced organic matter burial preservation. Difficulties associated with a tectonically driven model are discussed in Section 5.a.

Relatively short-lived negative excursions in the global marine $\delta^{13}C_{carb}$ record are achieved largely through transient perturbations to the carbon cycle, such as episodic changes in biological productivity (Zachos, Arthur & Dean, 1989; Kump, 1991), the rapid release of isotopically light carbon from gas hydrate sources (Dickens *et al*. 1995), sea-level change and associated variation in reduced carbon storage on continental shelves, and upwelling of a stratified ocean with anoxic deep-waters (Knoll *et al*. 1996). If related to productivity, excursions of the magnitude observed (2–3 ‰) would require the near cessation of productivity, similar to conditions associated with the Cretaceous–Tertiary extinction event (Kump, 1991). This mechanism seems unlikely when considered in light of the Mesoproterozoic fossil record (Knoll, 1992). The release of methane from gas hydrate sources is also an unsatisfactory explanation. Although relative to today the residence time of methane may have been significantly longer in the anoxic, SO_4-poor Proterozoic ocean (Pavlov *et al*. 2003), mass balance constraints indicate that the system will recover rapidly from an episodic injection of methane (Dickens, Castillo & Walker, 1997). As such, isotopic excursions associated with methane release are extremely abrupt and therefore difficult to identify in the ancient geological record, in particular where the sampling resolution is large (5–10 m for most Proterozoic records). In the Dismal Lakes Group, the excursions to lower $\delta^{13}C$ values occur near sequence boundaries, suggesting that the shifts are related to changes in sea level.

5.a. Invoking a tectonic explanation

The static nature of the early Mesoproterozoic carbon isotope record has been interpreted to reflect unusual stability in the carbon cycle controlled by low primary productivity during an interval of prolonged tectonic quiescence that resulted in nutrient stability and P-limitation in the oceans (Buick, Des Marais & Knoll, 1995; Brasier & Lindsay, 1998; Lindsay & Brasier, 2000). Higher $\delta^{13}C$ values observed in Neoproterozoic successions have been attributed to increased biological productivity and burial preservation of C_{org} (Des

Marais *et al*. 1992; Des Marais, 1994), perhaps triggered by higher sedimentation rates associated with the assembly of Gondwana (Knoll *et al*. 1986; Kaufman, Jacobsen & Knoll, 1993). A similar explanation has been invoked by Bartley *et al*. (2001) to explain the more recently recognized and relatively modest mid-Mesoproterozoic baseline shift to higher $\delta^{13}C$ values (this paper; Kah *et al*. 1999*a*). The timing of the shift ($\sim$1300 Ma) corresponds closely to a rise in marine $^{87}Sr/^{86}Sr$ ratios (Bartley *et al*. 2001) and a peak in arc formation (McLelland, Daly & McLelland, 1996), interpreted to mark the onset of Rodinia assembly.

Although attractive, a purely tectonic rationalization for the Mesoproterozoic carbon record remains unsatisfactory. P-limitation models, which rely on global tectonic quiescence to account for stasis in the marine $\delta^{13}C$ record prior to $\sim$1300 Ma (Buick, Des Marais & Knoll, 1995; Brasier & Lindsay, 1998; Lindsay & Brasier, 2000), are challenged by evidence for tectonic activity between $\sim$1900 and $\sim$1300 Ma (Hoffman, 1989; Karlstrom *et al*. 2001; Moores, 2002). Furthermore, evidence for continuously high rates of siliciclastic deposition between $\sim$1300 and 1000 Ma, necessary to sustain enhanced burial of C_{org}, is lacking. Rather, data from detrital zircons from the Neoproterozoic Shaler Supergroup and coeval successions (Rainbird, Heaman & Young, 1992; Khudoley *et al*. 2001) suggest that the most significant siliciclastic deposition occurred after $\sim$850 Ma, in association with rapid denudation of the Grenville orogen.

5.b. Evolutionary developments

Throughout the Proterozoic, complex communities of benthic prokaryotes, manifest as microbial mats, dominated carbonate platforms. Their restriction to shallow marine environments suggests that photosynthesis was the primary means of organic matter production for these benthic communities. Despite the abundance of photosynthetic prokaryotes, however, rapid consumption by oxidants (Canfield & Des Marais, 1993) and carbonate dilution likely resulted in very little burial preservation of C_{org} in association with microbialite-dominated carbonates of the Proterozoic (Des Marais, 1991). Palaeontological evidence indicates that the other dominant life forms, the photosynthetic eukaryotes, occurred in relatively low abundance and diversity prior to *c*. 1250 Ma (Summons & Walter, 1990; Knoll, 1992, 1994), with most forms inhabiting coastal environments (Javaux, Knoll & Walter, 2001). Beginning $\sim$1300 Ma, however, larger and more complex acritarchs with organic walls composed of more robust organic material became increasingly abundant (Knoll, 1994; Butterfield, 1997; Xiao *et al*. 1997). Through the remainder of the Proterozoic, modern groups of photosynthetic eukaryotes, including multicellular red and yellow-green algae (Butterfield, Knoll & Swett, 1990; Woods, Knoll & German, 1998; Butterfield, 2000), gradually expanded to inhabit previously unoccupied marine habitats (Butterfield & Chandler, 1992).

These patterns of eukaryotic diversification have been attributed to changes in the availability of biologically important trace metals (that is, Fe and Mo), which affected nitrogen fixation and nitrate assimilation in the Proterozoic ocean (Anbar & Knoll, 2002). The availability of dissolved forms of Fe and Mo may have been limited by the anoxic, and perhaps sulphidic, nature of the deep ocean (Canfield, 1998), which promoted the removal of these elements to sediments. Anbar & Knoll (2002) suggested that prior to $\sim$1250 Ma, eukaryotic algae preferred coastal and estuarine sites due to the proximity of these areas to nutrient and metal sources derived from rivers and upwelling-related processes on basin margins. Increased weathering and erosion at $\sim$1250 Ma associated with the onset of the Grenville Orogeny is suggested to have increased the supply of trace metals and phosphorus to the oceans (Anbar & Knoll, 2002). Furthermore, enhanced burial preservation of C_{org} with increased sedimentation rates may have led to a modest rise in atmospheric P_{O_2}. This postulated rise in P_{O_2} may be reflected in the rock record as the oldest, laterally extensive, bedded marine $CaSO_4$ evaporites preserved within the $\sim$1200 Ma Grenville and Bylot supergroups (Kah, Lyons & Chesley, 2001). With the rise in O_2, N-limitation may have lessened, stimulating productivity and facilitating eukaryotic diversification (Anbar & Knoll, 2002). Although increased erosion with the onset of the Grenville Orogeny may have increased sedimentation rates along basin margins and enhanced burial preservation of C_{org}, orogenic effects alone cannot fully explain the character of the mid-Mesoproterozoic transition in marine $\delta^{13}C$. Rather, we suggest that the evolutionary developments, triggered by increased nutrient and trace metal availability, played the larger role in shaping the carbon isotope evolution of the Mesoproterozoic ocean.

Palaeontological data indicate that prior to $\sim$1300–1250 Ma, most carbonate and organic matter accumulated in shallow marine environments due to the environmental limitations of eukaryotes and photosynthetic prokaryotes in benthic microbial mats (Grotzinger, 1990; Knoll, Fairchild & Swett, 1993; Kah & Knoll, 1996). Under these conditions, C_{carb} and C_{org} were exhumed simultaneously during sea level lowstands. Because secular variation in marine $\delta^{13}C$ is driven largely by changes in f_{org} (Kump & Arthur, 1999), this pairing of the two sedimentary carbon reservoirs limited variation in the marine $\delta^{13}C$ value throughout much of the Palaeoproterozoic and early Mesoproterozoic.

In the latter half of the Mesoproterozoic, eukaryotes became more abundant and diversified to inhabit open ocean sites. Thus, while carbonate sediments continued

to accumulate principally in shallow marine settings, sites of organic matter accumulation expanded to include the deep sea. An anoxic and possibly sulphidic deep ocean environment that may have persisted well into the Neoproterozoic (Canfield, 1998) would have promoted preservation of organic matter in deep-sea sediments (Canfield, 1994). An increase in f_{org} associated with sequestration of C_{org} in the deep sea would have produced an increase in the average $\delta^{13}C$ value of the ocean, recorded in the Mesoproterozoic record as a shift in the $\delta^{13}C_{carb}$ baseline from 0 to +3.5 ‰. Intermittent upwelling along basin margins, however, would mix ^{13}C-depleted deep waters with the shallow ocean. Subsequent oxidation of this carbon would cause a decrease in the $\delta^{13}C$ value of marine DIC (dissolved inorganic carbon), which would be reflected in the geological record as a transient decrease in $\delta^{13}C_{carb}$. In the Dismal Lakes Group, negative carbon isotope excursions occur in association with sequence boundaries, suggesting that upwelling during changing sea level may have played a role in transferring reduced carbon to the shallow ocean. The effectiveness of the oxidation process, echoed in the magnitude of negative isotopic excursions, would have intensified as the upper ocean and atmosphere became gradually more oxidizing due to increasing burial preservation of C_{org}. Despite the relatively high carbonate saturation state of the Proterozoic ocean (Grotzinger, 1989), which buffered the carbon isotope composition of marine DIC, an increasing contribution of isotopically light C_{org} would have gradually lowered the $\delta^{13}C$ value of ΣCO_2 in the deeper waters of the stratified ocean. Thus, as the deep sea became more depleted in ^{13}C, and the atmosphere became more oxidizing, upwelling events would have produced excursions in $\delta^{13}C_{carb}$ that became increasingly negative with time. Coupled with a long-term shift in $\delta^{13}C_{carb}$ due to increases in f_{org} and the crustal inventory of C_{org}, these changes would have yielded a marine system that became isotopically more variable with time, similar to the temporal trend observed in Mesoproterozoic–Neoproterozoic records. Patterns of secular variation typical of the Phanerozoic, generally marked by less extreme variation in $\delta^{13}C_{carb}$, would have been reached only as the ocean became less stratified, dissolved O_2 levels increased and processes of *in situ* organic matter oxidation in the deep sea became more efficient.

6. Conclusions

With the increased availability of well-constrained carbon isotope data, a clearer picture is emerging of the complex interactions among biogeochemical processes that shaped the interval leading up to the Neoproterozoic. We propose that increased storage of C_{org} in anoxic marine sites after ~1250 Ma led to the release of O_2 to Earth's surface environments. As oxygen levels in the atmosphere and shallow ocean increased, trace metals brought to the shallow ocean via rivers and upwelling were oxidized, easing nutrient restrictions that had previously limited eukaryotic algae to coastal and estuarine sites (Anbar & Knoll, 2002). Carbon isotope records suggest that these changes developed into a self-perpetuating system, wherein increasing C_{org} production and accumulation in the deep sea drove a steady, but gradual increase in $\delta^{13}C_{carb}$. At the same time, as the deep sea became increasingly depleted in ^{13}C and the atmosphere more oxidizing, reduced carbon brought to the surface ocean via upwelling produced excursions in $\delta^{13}C_{carb}$ that became progressively more negative. Coupled with the long-term increase in $\delta^{13}C_{carb}$ these changes resulted in a marine system that evolved to become isotopically more variable.

The hypothesis presented herein provides an explanation for carbon isotope patterns observed in Mesoproterozoic strata and is consistent with emerging models based on independent criteria (e.g. Anbar & Knoll, 2002). However, current understanding of how evolutionary changes, orogenic events and redox transitions combined to shape the Mesoproterozoic Earth remains somewhat unrefined due to limitations in available data. In particular, the lack of a robust chronostratigraphy for this critical interval makes it difficult to compare geographically distributed records and, as such, reduces the capacity of researchers to develop a clear global picture. Although significant progress is being made through the generation of $\delta^{13}C_{carb}$ records (this study; Kah *et al*. 1999*a*; Bartley *et al*. 2001) and emerging $\delta^{34}S$ records (Kah, Lyons & Chesley, 2001), the development of a robust Sr isotope stratigraphy for the Mesoproterozoic is necessary to provide further insight into relationships between global tectonic events, continental weathering and biological diversification and the effects of these relationships on the evolution of the Mesoproterozoic environment.

Acknowledgements. Research associated with the present study was supported by NSF Grants EAR-9725538 (TWL and LCK) and EAR-9725395 (TDF) and a grant to LCK from the National Geographic Society. We thank Air Tindi and Canada's Department of Indian and Northern Affairs for field logistical support, G. Ross for assistance in choosing field localities, J. Bartley, B. Thomas and M. Formolo for field assistance and thoughtful discussion, and M. Emmons for assistance with stable isotope analyses. Insightful comments from J. Kaufman and an anonymous reviewer helped to improve this manuscript.

References

AITKEN, J. & PUGH, D. 1984. The Fort Norman and Leith Ridge structures: major, buried, Precambrian features underlying Franklin Mountains and Great Bear and Mackenzie Plains. *Bulletin of Canadian Petroleum Geology* **32**, 139–46.

ANBAR, A. D. & KNOLL, A. H. 2002. Proterozoic ocean chemistry and evolution: a bioinorganic bridge? *Science* **297**, 1137–42.

ANDERSON, H. E. & DAVIS, D. W. 1995. U–Pb geochronology of the Moyie sills, Purcell Supergroup, southeastern British Columbia: implications for the Mesoproterozoic geological history of the Purcell (Belt) basin. *Canadian Journal of Earth Sciences* **32**, 1180–93.

BANNER, J. L. & HANSON, G. N. 1990. Calculation of simultaneous isotopic and trace element variations during water-rock interaction with applications to carbonate diagenesis. *Geochimica et Cosmochimica Acta* **54**, 3123–37.

BARAGER, W. R. A. & DONALDSON, J. A. 1973. Coppermine and Dismal Lakes Map Area. *Geological Survey of Canada, Paper* **71-39**, 20 pp.

BARTLEY, J. K., KNOLL, A. H., GROTZINGER, J. P. & SERGEEV, V. N. 2000. Lithification and fabric genesis in precipitated stromatolites and associated peritidal carbonates, Mesoproterozoic Billyakh Group, Siberia. In *Carbonate Sedimentation and Diagenesis in the Evolving Precambrian World* (eds J. P. Grotzinger and N. P. James), pp. 59–73. SEPM Special Publication no. 67.

BARTLEY, J. K., POPE, M., KNOLL, A. H., SEMIKHATOV, M. A. & PETROV, P. YU. 1998. A Vendian–Cambrian boundary succession from the northwestern margin of the Siberian Platform; stratigraphy, palaeontology, chemostratigraphy and correlation. *Geological Magazine* **135**, 473–94.

BARTLEY, J. K., SEMIKHATOV, M. A., KAUFMAN, A. J., KNOLL, A. H., POPE, M. C. & JACOBSEN, S. B. 2001. Global events across the Mesoproterozoic–Neoproterozoic boundary: C and Sr isotopic evidence from Siberia. *Precambrian Research* **111**, 165–202.

BOWRING, S. A. & ROSS, G. M. 1985. Geochronology of the Narakay volcanic complex: Implications for the age of the Coppermine Homocline and Mackenzie igneous events. *Canadian Journal of Earth Sciences* **22**, 774–80.

BRAND, U. & VEIZER, J. 1980. Chemical diagenesis of a multicomponent carbonate system – 1) Trace elements. *Journal of Sedimentary Petrology* **50**, 1219–36.

BRASIER, M. D., GREEN, O. & SHIELDS, G. 1997. Ediacarian sponge spicule clusters from southwestern Mongolia and the origins of the Cambrian fauna. *Geology* **25**, 303–6.

BRASIER, M. D. & LINDSAY, J. F. 1998. A billion years of environmental stability and the emergence of eukaryotes: New data from northern Australia. *Geology* **26**, 555–8.

BRASIER, M. D., SHIELDS, G., KULESHOV, V. N. & ZHEGALLO, L. A. 1996. Integrated chemo- and biostratigraphic calibration of early animal evolution: Neoproterozoic–early Cambrian of southwest Mongolia. *Geological Magazine* **133**, 445–85.

BUICK, R., DES MARAIS, D. & KNOLL, A. H. 1995. Stable isotope compositions of carbonates from the Mesoproterozoic Bangemall Group, Australia. *Chemical Geology* **123**, 153–71.

BUTTERFIELD, N. J. 1997. Plankton ecology and the Proterozoic–Phanerozoic transition. *Paleobiology* **23**, 247–62.

BUTTERFIELD, N. J. 2000. *Bangiomorpha pubescens* n. gen., n. sp.: implications for the evolution of sex, multicellularity, and the Mesoproterozoic/Neoproterozoic radiation of eukaryotes. *Paleobiology* **26**, 386–404.

BUTTERFIELD, N. J. & CHANDLER, F. W. 1992. Palaeoenvironmental distribution of Proterozoic microfossils, with an example from the Agu Bay Formation, Baffin Island. *Palaeontology* **35**, 943–57.

BUTTERFIELD, N. J., KNOLL, A. H. & SWETT, K. 1990. A bangiophyte red alga from the Proterozoic of Arctic Canada. *Science* **250**, 104–7.

CAMPBELL, F. H. A. 1978. Geology of the Helikian rocks of the Bathurst Inlet area, Northwest Territories. *Geological Survey of Canada, Paper* **78-1A**, 97–106.

CANFIELD, D. E. 1989. Sulfate reduction and oxic respiration in marine sediments; implications for organic carbon preservation in euxinic environments. *Deep-Sea Research. Part A: Oceanographic Research Papers* **36**(1a), 121–38.

CANFIELD, D. E. 1994. Factors influencing organic carbon preservation in marine sediments. *Chemical Geology* **114**, 315–29.

CANFIELD, D. E. 1998. A new model for Proterozoic ocean chemistry. *Nature* **396**, 450–3.

CANFIELD, D. E. & DES MARAIS, D. J. 1993. Biogeochemical cycles of carbon, sulfur, and free oxygen in a microbial mat. *Geochimica et Cosmochimica Acta* **57**, 3971–84.

CANFIELD, D. E. & TESKE, A. 1996. Late Proterozoic rise in atmospheric oxygen concentration inferred from phylogenetic and sulphur-isotope studies. *Nature* **382**, 127–32.

CARPENTER, S. J., LOHMANN, K. C., HOLDEN, P., WALTER, L. M., HUSTON, T. J. & HALLIDAY, A. N. 1991. $\delta^{18}O$ values, $^{87}Sr/^{86}Sr$ and Sr/Mg ratios of Late Devonian marine calcite: Implications for the composition of ancient seawater. *Geochimica et Cosmochimica Acta* **55**, 1991–2010.

CHOQUETTE, P. W. & JAMES, N. P. 1990. Limestones – the burial diagenetic environment. In *Diagenesis* (eds I. A. McIlreath and D. W. Morrow), pp. 75–111. *Geoscience Canada Reprint Series* **4**.

COOK, D. G. & MACLEAN, B. C. 1992. Proterozoic thick-skinned intracratonic deformation, Colville Hills region, Northwest Territories, Canada. *Geology* **20**, 67–70.

COOK, D. G. & MACLEAN, B. C. 1995. The intracratonic Palaeoproterozoic Forward orogeny, and implications for regional correlations, Northwest Territories, Canada. *Canadian Journal of Earth Sciences* **32**, 1991–2008.

COOK, D. G. & MACLEAN, B. C. 1996. Mid-continent tectonic inversions, Northwest Territories, Canada. *Journal of Structural Geology* **18**, 791–802.

COOK, F. A. & TAYLOR, G. G. 1991. Seismic reflection trace synthesized from Proterozoic outcrop and its correlation to seismic profiles in northwestern Canada. *Tectonophysics* **191**, 111–26.

CRAIG, H. 1957. Isotopic standards for carbon and oxygen and correction factors for mass-spectrometric analysis of carbon dioxide. *Geochimica et Cosmochimica Acta* **12**, 133–49.

DALZIEL, I. W. D. 1991. Pacific margins of Laurentia and East Antarctica–Australia as a conjugate rift pair: evidence and implications for an Eocambrian supercontinent. *Geology* **19**, 598–601.

DEMAISON, G. J. & MOORE, G. T. 1980. Anoxic environments and oil source bed genesis. *American Association of Petroleum Geologists Bulletin* **64**(8), 1179–1209.

DES MARAIS, D. J. 1991. Microbial mats, stromatolites and the rise of oxygen in the Precambrian atmosphere. *Global and Planetary Change* **5**, 93–6.

DES MARAIS, D. J. 1994. Tectonic control of the crustal organic carbon reservoir during the Precambrian. *Chemical Geology* **114**, 303–14.

DES MARAIS, D. J. 1997. Isotopic evolution of the biogeochemical carbon cycle during the Proterozoic Eon. *Organic Geochemistry* **27**, 185–93.

DES MARAIS, D. J., STRAUSS, H., SUMMONS, R. E. & HAYES, J. M. 1992. Carbon isotope evidence for the stepwise oxidation of the Proterozoic environment. *Science* **359**, 605–9.

DICKENS, G. R., CASTILLO, M. M. & WALKER, J. C. G. 1997. A blast of gas in the latest Paleocene; simulating first-order effects of massive dissociation of oceanic methane hydrate. *Geology* **25**(3), 259–62.

DICKENS, G. R., O'NEIL, J. R., REA, D. K. & OWEN, R. M. 1995. Dissociation of oceanic methane hydrate as a cause of the carbon isotope excursion at the end of the Paleocene. *Paleoceanography* **10**, 965–71.

DONALDSON, J. A. 1976. Palaeoecology of conophyton and associated stromatolites in the Precambrian Dismal Lakes and Rae groups, Canada. In *Stromatolites, Developments in Sedimentology 20* (ed. M. R. Walter), pp. 523–34. Amsterdam: Elsevier.

DOUGHTY, P. T. & CHAMBERLAIN, K. R. 1996. Salmon River Arch revisited: new evidence for 1370 Ma rifting near the end of deposition in the Middle Proterozoic Belt basin. *Canadian Journal of Earth Sciences* **33**, 1037–52.

FAIRCHILD, I. J., MARSHALL, J. D. & BERTRAND-SARFATI, J. 1990. Stratigraphic shifts in carbon isotopes from Proterozoic stromatolitic carbonates (Mauritania); influences of primary mineralogy and diagenesis. *American Journal of Science* **290-A**, 46–79.

FEDONKIN, M. A. 1990. Major events in the history of India: Precambrian metazoans. In *Palaeobiology: A Synthesis* (eds D. E. G. Briggs and P. R. Crowther), pp. 132–7. Bristol: University of Bristol.

FRANK, T. D. & LYONS, T. W. 2000. The integrity of $\delta^{18}O$ records in Precambrian carbonates: a Mesoproterozoic case study. In *Carbonate sedimentation and diagenesis in the evolving Precambrian world* (eds J. P. Grotzinger and N. P. James), pp. 315–26. SEPM Special Publication no. 67.

FRANK, T. D., LYONS, T. W. & LOHMANN, K. C 1997. Isotopic evidence for the paleoenvironmental evolution of the Mesoproterozoic Helena Formation, Belt Supergroup, Montana. *Geochimica et Cosmochimica Acta* **61**, 5023–41.

GHAZBAN, F., SCHWARTZ, H. P. & FORD, D. C. 1992. Multistage dolomitization in the Society Cliffs Formation, northern Baffin Island, Northwest Territories, Canada. *Canadian Journal of Earth Sciences* **29**, 1459–73.

GROTZINGER, J. P. 1989. Facies and evolution of Precambrian depositional systems: emergence of the modern platform archetype. In *Controls on Carbonate Platform and Basin Development* (eds P. D. Crevello, J. J. Wilson, J. F. Sarg and J. F. Read), pp. 79–106. SEPM Special Publication no. 44.

GROTZINGER, J. P. 1990. Geochemical model for Proterozoic stromatolite decline. *American Journal of Science* **290-A**, 80–103.

GROTZINGER, J. P., BOWRING, S. A., SAYLOR, B. Z. & KAUFMAN, A. J. 1995. Biostratigraphic and geochronologic constraints on early animal evolution. *Science* **270**, 598–604.

GROTZINGER, J. P., WATTERS, W. A. & KNOLL, A. H. 2000. Calcified metazoans in thrombolite-stromatolite reefs of the terminal Proterozoic Nama Group, Namibia. *Paleobiology* **26**, 334–59.

HILDEBRAND, R. 1981. Early Proterozoic Labine Group of Wopmay Orogen: remnant of a continental volcanic arc developed during oblique convergence. In *Proterozoic Basins of Canada* (ed. F. H. A. Campbell), pp. 133–56. Geological Survey of Canada, Paper 81-10.

HOFFMAN, P. F. 1980*a*. Conjugate transcurrent faults in north-central Wopmay Orogen (early Proterozoic) and their dip-slip reactivation during post-orogenic extension, Hepburn Lake map area, District of Mackenzie. *Geological Survey of Canada, Paper* **80-1A**, 183–5.

HOFFMAN, P. F. 1980*b*. On the relative age of the Muskox intrusion and the Coppermine River basalts, District of Mackenzie. *Geological Survey of Canada, Paper* **80-1A**, 223–5.

HOFFMAN, P. F. 1989. Speculations on Laurentia's first gigayear (2.0 to 1.0 Ga). *Geology* **17**, 135–8.

HOFFMAN, P. F. 1991. Did the breakout of Laurentia turn Gondwanaland inside-out? *Science* **252**, 1409–12.

HOFFMAN, P. F. & BOWRING, S. A. 1984. Short-lived 1.9 Ga continental margin and its destruction, Wopmay orogen, northwest Canada. *Geology* **12**, 68–72.

HOFFMAN, P. F., KAUFMAN, A. J. & HALVERSON, G. P. 1998. Comings and goings of global glaciations on a Neoproterozoic tropical platform in Namibia. *GSA Today* **8**, 1–9.

HOFFMAN, P. F., KAUFMAN, A. J., HALVERSON, G. P. & SCHRAG, D. P. 1998. A Neoproterozoic snowball Earth. *Science* **281**, 1342–6.

HOFFMAN, P. F. & ST-ONGE, M. R. 1981. Contemporaneous thrusting and conjugate transcurrent faulting during the second collision in Wopmay Orogen: implications for the subsurface structure if post-orogenic outliers. *Geological Survey of Canada, Paper* **80-1A**, 251–7.

HOFMANN, H. J. & JACKSON, G. D. 1991. Shelf-facies microfossils from the Uluksan Group (Proterozoic Bylot Supergroup), Baffin Island, Canada. *Journal of Paleontology* **65**, 361–82.

HOLLAND, H. D. 1984. *The chemical evolution of the atmosphere and oceans.* Princeton, NJ: Princeton University Press, 582 pp.

HORODYSKI, R. J. & DONALDSON, J. A. 1980. Microfossils from the Middle Proterozoic Dismal Lakes Group, Arctic Canada. *Precambrian Research* **11**, 125–59.

HORODYSKI, R. J. & DONALDSON, J. A. 1983. Distribution and significance of microfossils in cherts of the Middle Proterozoic Dismal Lakes Group, District of Mackenzie, Northwest Territories, Canada. *Journal of Paleontology* **57**, 271–88.

IRVINE, T. N. 1970. Crystallization sequences in the Muskox intrusion and other layered intrusions, I. Olivine-pyroxene-plagioclase relations. *Geological Society of South Africa, Special Publication* **1**, 441–76.

JAVAUX, E. J., KNOLL, A. H. & WALTER, M. R. 2001. Morphological and ecological complexity in early eukaryotic ecosystems. *Nature* **412**, 66–9.

KAH, L. C. 2000. Preservation of depositional $\delta^{18}O$ signatures in Proterozoic dolostones: Geochemical constraints on seawater chemistry and early diagenesis. In *Carbonate sedimentation and diagenesis in the evolving Precambrian world* (eds J. P. Grotzinger and N. P. James), pp. 345–60. SEPM Special Publication no. 67.

KAH, L. C. & BARTLEY, J. K. 1997. Establishing a carbon isotopic reference curve for the Mesoproterozoic: Biogeochemical links to the tectonic assembly of Rodinia: *Geological Society of America, Abstracts with Programs* **29**, A-115.

KAH, L. C., BARTLEY, J. K., FRANK, T. D. & LYONS, T. W. 1999*b*. Reef facies and possible chemosynthetic communities of the Sulky formation, ~1.3 Ga Dismal Lakes Group, NWT, Canada. *Geological Association of Canada/Mineralogical Association of Canada, Joint Annual Meeting Abstracts* **24**, 60.

KAH, L. C. & KNOLL, A. H. 1996. Microbenthic distribution in Proterozoic tidal flats: Environmental and taphonomic considerations. *Geology* **24**, 79–82.

KAH, L. C., LYONS, T. W. & CHESLEY, J. T. 2001. Geochemistry of a 1.2 Ga carbonate–evaporite succession, northern Baffin and Bylot Islands: implications for Mesoproterozoic marine evolution. *Precambrian Research* **111**, 203–34.

KAH, L. C., SHERMAN, A. G., NARBONNE, G. M., KNOLL, A. H. & KAUFMAN, A. J. 1999*a*. $\delta^{13}C$ isotope stratigraphy of the Mesoproterozoic Bylot Supergroup, northern Baffin Island: Implications for regional lithostratigraphic correlations. *Canadian Journal of Earth Sciences* **36**, 313–32.

KARHU, J. A. & HOLLAND, H. D. 1996. Carbon isotopes and the rise of atmospheric oxygen. *Geology* **24**, 867–70.

KARLSTROM, K. E., ÅHALL, K. -I., HARLAN, S. S., WILLIAMS, M. L., MCLELLAND, J. & GEISSMAN, J. W. 2001. Long-lived (1.8–1.0 Ga) convergent orogen in southern Laurentia, its extensions to Australia and Baltica, and implications for refining Rodinia. *Precambrian Research* **111**, 5–30.

KAUFMAN, A. J., HAYES, J. M., KNOLL, A. H. & GERMS, G. J. B. 1991. Isotopic compositions of carbonates and organic carbon from upper Proterozoic successions in Namibia: stratigraphic variation and the effects of diagenesis and metamorphism. *Precambrian Research* **49**, 301–27.

KAUFMAN, A. J., JACOBSEN, S. B. & KNOLL, A. H. 1993. The Vendian record of Sr and C isotopic variations in seawater: Implications for tetonics and paleoclimate. *Earth and Planetary Science Letters* **120**, 409–30.

KAUFMAN, A. J. & KNOLL, A. H. 1995. Neoproterozoic variations in the C-isotopic composition of seawater; stratigraphic and biogeochemical implications. *Precambrian Research* **73**, 27–49.

KAUFMAN, A. J., KNOLL, A. H. & NARBONNE, G. M. 1997. Isotopes, ice ages, and terminal Proterozoic earth history. *Proceedings of the National Academy of Sciences* **94**, 6600–5.

KAUFMAN, A. J., KNOLL, A. H., SEMIKHATOV, M. A., GROTZINGER, J. P., JACOBSEN, S. B. & ADAMS, W. 1996. Integrated chronostratigraphy of Proterozoic–Cambrian boundary beds in the western Anabar Region, northern Siberia. *Geological Magazine* **133**, 509–33.

KENNEDY, M. J. 1996. Stratigraphy, sedimentology, and isotopic geochemistry of Australian Neoproterozoic postglacial cap dolostones: deglaciation, $\delta^{13}C$ excursions, and carbonate precipitation. *Journal of Sedimentary Research* **66**, 1050–64.

KERANS, C. 1983. Timing of emplacement of the Muskox intrusions: constraints from Coppermine Homocline cover strata. *Canadian Journal of Earth Sciences* **20**, 673–83.

KERANS, C. & DONALDSON, J. A. 1988. Proterozoic paleokarst profile, Dismal lakes Group, N.W.T., Canada. In *Paleokarst* (eds N. P. James and P. W. Choquette), pp. 167–82. New York: Springer-Verlag.

KERANS, C. & DONALDSON, J. A. 1989. Deepwater conical stromatolite reef, Sulky Formation (Dismal Lakes Group), Middle Proterozoic, N.W.T. In *Reefs, Canada and Adjacent Area* (eds H. H. J. Geldsetzer, N. P. James and G. E. Tebutt), pp. 81–8. Canadian Society of Petroleum Geologists, Memoir no. 13.

KERANS, C., ROSS, G. M., DONALDSON, J. A. & GELDSETZER, H. J. 1981. Tectonism and depositional history of the Helikian Hornby Bay and Dismal Lakes groups, District of Mackenzie. In *Proterozoic Basins of Canada* (ed. F. H. A. Campbell), pp. 157–82. Geological Survey of Canada, Paper 81-10.

KHUDOLEY, A. K., RAINBIRD, R. H., STERN, R. A., KROPACHEV, A. P., HEAMAN, L. M., ZANIN, A. M., PODKOVYROV, V. N., BELOVA, V. N. & SUKHORUKOV, V. I. 2001. Sedimentary evolution of the Riphean–Vendian basin of southeastern Siberia. *Precambrian Research* **111**, 129–63.

KNOLL, A. H. 1992. The early evolution of eukaryotes: a geological perspective. *Science* **256**, 622–7.

KNOLL, A. H. 1994. Proterozoic and Early Cambrian protists: evidence for accelerating evolutionary tempo. *Proceedings, National Academy of Science* **91**, 6743–50.

KNOLL, A. H., BAMBACH, R. K., CANFIELD, D. E., & GROTZINGER, J. P. 1996. Comparative Earth history and Late Permian mass extinction. *Science* **273**, 452–7.

KNOLL, A. H., FAIRCHILD, I. J. & SWETT, K. 1993. Calcified microbes in Neoproterozoic carbonates: implications for our understanding of the Proterozoic/Cambrian transition. *Palaios* **8**, 512–25.

KNOLL, A. H., HAYES, J. M., KAUFMAN, A. J., SWETT, K. & LAMBERT, I. B. 1986. Secular variation in carbon isotope ratios from Upper Proterozoic successions of Svalbard and East Greenland. *Nature* **321**, 832–8.

KNOLL, A. H., KAUFMAN, A. J. & SEMIKHATOV, M. A. 1995. The carbon isotopic composition of Proterozoic carbonates: Riphean successions from northwestern Siberia (Anabar Massif, Turukhansk Uplift). *American Journal of Science* **295**, 823–50.

KNOLL, A. H. & SERGEEV, V. N. 1995. Taphonomic and evolutionary changes across the Mesoproterozoic–Neoproterozoic boundary. *Neues Jahrbuch für Geologie und Paläontologie* **195**, 289–302.

KNOLL, A. H. & SWETT, K. 1990. Carbonate deposition during the late Proterozoic era: an example from Spitsbergen. *American Journal of Science* **290-A**, 104–32.

KNOLL, A. H. & WALTER, M. R. 1992. Latest Proterozoic stratigraphy and Earth history. *Nature* **136**, 673–8.

KUMP, L. R. 1991. Interpreting carbon-isotope excursions: Strangelove oceans. *Geology* **19**, 299–302.

KUMP, L. R. & ARTHUR, M. A. 1999. Interpreting carbon-isotope excursions; carbonates and organic matter. *Chemical Geology* **161**, 181–98.

LAMBERT, I. B., WALTER, M. R., WENLONG, Z., SONGNIAN, L. & GUOGAN, M. 1987. Palaeoenvironment and carbon isotope stratigraphy of Upper Proterozoic carbonates of the Yangtze Platform. *Nature* **325**, 140–2.

LECHEMINANT, A. N. & HEAMAN, L. M. 1989. Mackenzie igneous events, Canada: Middle Proterozoic hotspot magmatism associated with ocean opening. *Earth and Planetary Science Letters* **96**, 38–48.

LUEPKE, & LYONS, T. W. 2001. Pre-Rodinian (Mesoproterozoic) supercontinental rifting along the western margin of Laurentia; geochemical evidence from the Belt-Purcell Supergroup. *Precambrian Research* **111**, 79–90.

LINDSAY, J. F. & BRASIER, M. D. 2000. A carbon isotope reference curve for ca. 1700–1575 Ma, McArthur and Mount Isa Basins, Northern Australia. *Precambrian Research* **99**, 271–308.

LOHMANN, K. C. 1988. Geochemical patterns of meteoric diagenetic systems and their application to studies of paleokarst. In *Paleokarst* (eds N. P. James and P. W. Choquette), pp. 58–80. Springer-Verlag.

MAGARITZ, M., KIRSCHVINK, J. L., LATHAM, A. J., ZHURAVLEV, A. Y. & ROZANOV, A. Y. 1991. Precambrian/Cambrian boundary problem: Carbon isotope correlations for Vendian and Tommotian time between Siberia and Morocco. *Geology* **19**, 847–50.

MCLELLAND, J., DALY, J. S. & MCLELLAND, J. M. 1996. The Grenville orogenic cycle (ca. 1350–1000 Ma); an Adirondack perspective. *Tectonophysics* **265**, 1–28.

MOORES, E. M. 2002. Pre-1 Ga (pre-Rodinian) ophiolites; their tectonic and environmental implications. *Geological Society of America Bulletin* **114**, 80–95.

NARBONNE, G. M. 1998. The Ediacara biota: a terminal Neoproterozoic experiment in the evolution of life. *GSA Today* **8**, 1–6.

NARBONNE, G. M., KAUFMAN, A. J. & KNOLL, A. H. 1994. Integrated chemostratigraphy and biostratigraphy of the upper Windermere Supergroup, northwestern Canada: Implications for Neoproterozoic correlations and the early evolution of animals. *Geological Society of America Bulletin* **106**, 1281–92.

PARRISH, R. R. & BELL, R. T. 1987. Age of the NOR Breccia Pipe, Wernecke Supergroup, radiogenic age and isotopic studies. *Geological Survey of Canada, Paper* **87-2**, 3–42.

PAVLOV, A. A., HURTGEN, M. T., KASTING, J. F. & ARTHUR, M. A. 2003. Methane-rich Proterozoic atmosphere? *Geology* **31**, 87–90.

PELECHATY, S. M., JAMES, N. P., KERANS, C. & GROTZINGER, J. P. 1991. A middle Proterozoic palaeokarst unconformity and associated sedimentary rocks; Elu Basin, Northwest Canada. *Sedimentology* **38**, 775–97.

PELECHATY, S. M., KAUFMAN, A. J. & GROTZINGER, J. P. 1996. Evaluation of $\delta^{13}C$ isotope stratigraphy for intrabasinal correlation: Vendian strata of northeast Siberia. *Geological Society of America Bulletin* **108**, 992–1003.

RAINBIRD, R. H., HEAMAN, L. M. & YOUNG, G. M. 1992. Sampling Laurentia; detrital zircon geochronology offers evidence for an extensive Neoproterozoic river system originating from the Grenville Orogen. *Geology* **20**, 351–4.

RAINBIRD, R. H., JEFFERSON, C. W., HILDEBRAND, R. S. & WORTH, J. K. 1994. The Shaler Supergroup and revision of Neoproterozoic stratigraphy in Amundsen Basin, Northwest Territories. *Geological Survey of Canada, Paper* **1994-C**, 61–70.

RAINBIRD, R. H., JEFFERSON, C. W. & YOUNG, G. M. 1996. The early Neoproterozoic sedimentary Succession B of northwestern Laurentia: Correlations and palaeogeographic significance. *Geological Society of America Bulletin* **108**, 454–70.

ROSS, G. M. 1982. The Narakay Volcanic Complex: mafic volcanism in the Helikian Hornby Bay Group of Dease Arm, Great Bear Lake – a preliminary report on depositional processes and tectonic significance. *Geological Survey of Canada, Paper* **82-1A**, 329–40.

ROSS, G. M. & KERANS, C. 1988. *Geology of the Hornby Bay and Dismal Lakes groups, Coppermine Homocline, District of Mackenzie, Northwest Territories*. Geological Survey of Canada, Map 1663A, 1:250,000.

ROTHS, P. J. 1993. Geochemical and geochronological studies of the Grenville-age (1250–1000 Ma) Allamoore and Hazel Formations, Hudspeth and Culberson Counties, West Texas. In *Precambrian geology of Franklin Mountains and Van Horn Area, Trans-Pecos, Texas* (eds K. Soegaard, K. C. Nielsen, K. Marsaglia, C. Barnes, P. Roths, D. P. Elston and G. A. Clough), pp. 11–35. Denver: Geological Society of America.

SERGEEV, V. N. 1994. Microfossils in cherts from the Middle Riphean (Mesoproterozoic) Avzyan Formation, southern Ural Mountains, Russian Federation. *Precambrian Research* **65**, 231–54.

SERGEEV, V. N., KNOLL, A. H. & GROTZINGER, J. P. 1995. Palaeobiology of the Mesoproterozoic Billyakh Group, northern Siberia. *Palaeontological Society Memoir* **39**, 1–37.

SERGEEV, V. N., KNOLL, A. H., KOLOSOVA, S. P. & KOLOSOV, P. N. 1994. Microfossils in cherts from the Mesoproterozoic (Middle Riphean) Debengda Formation, the Olenek Uplift, Northeastern Siberia. *Stratigraphy and Geological Correlation* **2**, 19–33.

STRAUSS, H., DES, M. D. J., HAYES, J. M. & SUMMONS, R. E. 1992. The carbon-isotopic record. In *The Proterozoic biosphere; a multidisciplinary study* (eds W. Schopf and C. Klein), pp. 117–27. Cambridge University Press.

SUMMONS, R. E. & WALTER, M. R. 1990. Molecular fossils and microfossils of prokaryotes and protists from Proterozoic sediments. *American Journal of Science* **290-A**, 212–44.

SUMNER, D. Y. 1997. Late Archean calcite-microbe interactions: Two morphologically distinct microbial communities that affected calcite nucleation differently. *Palaios* **12**, 302–18.

SUMNER, D. Y. & GROTZINGER, J. P. 1996*a*. Herringbone calcite: Petrography and environmental significance. *Journal of Sedimentary Research* **66**, 419–29.

SUMNER, D. Y. & GROTZINGER, J. P. 1996*b*. Were kinetics of Archean calcium carbonate precipitation related to oxygen concentration? *Geology* **24**, 119–22.

VALLEY, J. W. 1986. Stable isotope geochemistry of metamorphic rocks. In *Stable Isotopes in High Temperature Geological Processes* (eds J. W. Valley, H. P. Taylor and J. R. O'Neil), pp. 445–90. *Reviews in Mineralogy* **16**.

VAN SCHMUS, W. R. & BOWRING, S. A. 1980. Chronology of igneous events in the Wopmay Orogen, Northwest Territories, Canada. *Geological Society of America, Abstracts with Programs* **12**, 540.

VEIZER, J. 1983. Trace elements and isotopes in sedimentary carbonates. *Reviews in Mineralogy* **11**, 265–300.

WOODS, K., KNOLL, A. H. & GERMAN, T. 1998. Xanthophyte algae from the Mesoproterozoic/Neoproterozoic transition: confirmation of evolutionary implications. *Geological Society of America Abstracts with Programs* **30**, A-232.

XIAO, S., KNOLL, A. H., KAUFMAN, A. J., YIN, L. & ZHANG, Y. 1997. Neoproterozoic fossils in Mesoproterozoic

rocks? Chemostratigraphic resolution of a biostratigraphic conundrum from the North China Platform. *Precambrian Research* **84**, 197–220.

XIAO, S., KNOLL, A. H. & YUAN, X. 1998. Morphological reconstruction of *Miaohephyton bifurcatum*, a possible brown alga from the Neoproterozoic Duoshantuo Formation, South China. *Journal of Paleontology* **72**, 1072–86.

XIAO, S., ZHANG, Y. & KNOLL, A. H. 1998. Three-dimensional preservation of algae and animal embryos in a Neoproterozoic phosphorite. *Nature* **391**, 553–8.

YOUNG, G. M. 1979. Correlation of middle and upper Proterozoic strata of the northern rim of the North Atlantic craton. *Transactions of the Royal Society of Edinburgh* **70**, 323–36.

YOUNG, G. M. 1981*a*. Upper Proterozoic supracrustal rocks of North America: a brief review. *Precambrian Research* **15**, 305–30.

YOUNG, G. M. 1981*b*. The Amundsen Embayment, Northwest Territories; relevance to the Upper Proterozoic evolution of North America. In *Proterozoic Basins of Canada* (ed. F. H. A. Campbell), pp. 203–18. Geological Survey of Canada, Paper 81-10.

ZACHOS, J. C., ARTHUR, M. A., & DEAN, W. E. 1989. Geochemical evidence for suppression of pelagic marine productivity at the Cretaceous/Tertiary boundary. *Nature* **337**, 61–4.

ZHANG, Y. & YUAN, X. 1996. Sexual reproductive structures of Latest Proterozoic multicellular rhodophytes (red algae) from South China. *Science in China, Series C, Life Sciences* **39**, 28–36.